Accepted Manuscript

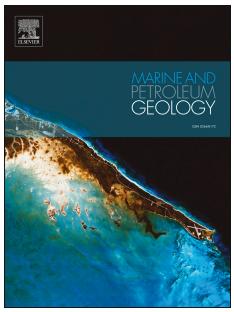

Mass transfer between sandstones and interbedded mudstones: Impact on petroleum charge, Bohai Bay Basin, China

Hongjin Hu, Youlu Jiang, Jon Gluyas, Kai Zhao, Jianjun Fang, Yu Wang, Yunqian Lu

PII: S0264-8172(19)30204-1

DOI: https://doi.org/10.1016/j.marpetgeo.2019.05.007

Reference: JMPG 3827

To appear in: *Marine and Petroleum Geology*

Received Date: 22 December 2018

Revised Date: 16 March 2019

Accepted Date: 7 May 2019

Please cite this article as: Hu, H., Jiang, Y., Gluyas, J., Zhao, K., Fang, J., Wang, Y., Lu, Y., Mass transfer between sandstones and interbedded mudstones: Impact on petroleum charge, Bohai Bay Basin, China, *Marine and Petroleum Geology* (2019), doi: https://doi.org/10.1016/j.marpetgeo.2019.05.007.

Mass transfer between sandstones and interbedded mudstones: impact on petroleum charge, Bohai Bay Basin, China

Hongjin HU [a,b], Youlu JIANG [a], Jon GLUYAS [b], Kai ZHAO [a,b], Jianjun FANG [c], Yu WANG [a], Yunqian LU [a]

a School of Geoscience, China University of Petroleum, Qingdao, 266580, China
b Department of Earth sciences, Durham University, Durham, DH1 3LE, UK
c Research Institute of Petroleum Exploration and Development, Shengli Oilfield Company, SINOPEC, Dongying City, Shandong Province, 257015, China

Abstract: The Permo-Carboniferous sandstones in the Gubei area, Bohai Bay Basin, are reservoirs for large accumulations of natural gas. The natural gas accumulations only occur in the sandstone beds thicker than 1.9m. Moreover, the maximum porosity of every bed correlates positively with bed thickness up to 2.0m and for thicker beds porosity is uniform. Porosity transitional zones developed at the top and bottom of each bed, with mean thicknesses of 1.25m and 0.75 m, respectively. Porosity shows a positive correlation with the distance to the sandstone/mudstone contact in the zones.

Interpretations based upon an extensive petrographic and geochemical database indicate that the sandstones experienced a mass fluid input from the adjacent mudstones during the early diagenesis. The infiltration resulted in extensive clay coats and pore-filling cements in sandstones, which were effective for inhibiting dissolution of grains during subsequent diagenesis process. The mass introduction only affected the marginal parts of the sandstones within 1.25 m of the top and 0.75m of the bottom of every bed, causing thin sandstone beds with thickness of approximately 2m to be tightly cemented totally. Thus the central parts of each (thicker) beds became preferential sites for the natural gas accumulation.

The differential levels of cementation in thin and thick sandstone beds observed here has

significant implications for exploration of similar interbedded sandstone and shale sequences elsewhere including shale gas targets.

Keywords: Sandstone diagenesis; Reservoir quality; Diagenetic mass transfer; Hydrocarbon differential filling; Carboniferous-Permian system; Gubei Gas Field; Bohai Bay Basin

1. Introduction

Permo-Carboniferous sandstones are one of the main objectives for deep hydrocarbon exploration in Bohai Bay Basin (Song et al, 2013). Many oil and gas deposits with large reserves, such as Suqiao-Wen'an gas field in Jizhong Depression (Liu et al, 2017), Gubei gas field in Jiyang Depression (Zhang et al., 2009), and Hugu 2 gas field in Linqing Depression (Li et al., 2015) occur in these sandstones. A key exploration issue for these sandstone reservoirs is that the stacked sandstone beds of the strata are variably hydrocarbon-bearing and water-bearing, although the sedimentary setting of all sand beds is similar and petroleum migration pathways are also similar. The failure rate for exploration of hydrocarbons in Permo-Carboniferous sandstones remains high due to the inaccurate predictions on the heterogeneity of hydrocarbon distribution. Reservoir quality is the most direct factor on hydrocarbon distribution (Morad et al., 2010; Taylor et al.,2010; Lai et al., 2017b; Lai et al., 2018). Diagenesis, consisting of mechanical compaction and chemical dissolution, precipitation and alteration, progressively alters reservoir quality during burial (Dutton et al, 2010; Bjørlykke and Jahren, 2012; Bjørlykke, K., 2014; Yuan et al, 2015; Gluyas & Yuan, 2018).

The Gubei area is one of the main areas in the Bohai Basin for the exploration of the Permo-Carboniferous gas play. To date the proven natural gas reserves are 68×10^8 m^3 (Zhang

et al., 2009), however the exploration success rate is only 50% when drilling on valid closures.

The Permo-Carboniferous sandstone reservoirs in Jiyang sub-basin have been studied in order to understand the controls on gas accumulation. The objectives of this study were to: (1) report the heterogeneity characteristic of natural gas distribution and reservoir quality; (2) investigate the differential diagenesis, reconstruct diagenetic and reservoir quality evolution history of the Permo-Carboniferous sandstones; (3) analyze the links among reservoir diagenesis, reservoir quality evolution and hydrocarbon differential filling in temporal scale and ultimately to develop a model for forecasting reservoir quality ahead of drilling.

2. Geological Setting

The Gubei area is a NE-dipping buried hill between Gubei sag and Bonan sag in the east of Zhanhua Depression, Jiyang Sub-basin (Fig. 1).

From Paleozoic to the Cenozoic, the Gubei area has undergone multiple tectonic events. The Permo-Carboniferous strata experience three burial episodes in the Paleozoic-Middle Triassic, Jurassic-Middle Cretaceous and Cenozoic, respectively, and two uplift episodes of in the Late Triassic and Late Cretaceous (Peng et al., 2010). The uplift movements in the Late Triassic led to significant erosion of Permo-Carboniferous, while the uplift that occurred in Late Cretaceous did not (Fig.2) (Peng et al., 2010).

Sediments accumulated in the Gubei area comprise Ordovician carbonate platform deposits overlain by Permo-Carboniferous transitional marine-terrestrial deposits. Younger strata included terrestrial clastics, volcaniclastics and lacustrine deposits (Fig.3). The boundaries between Ordovician and Permo-Carboniferous, Permian and Mesozoic, Mesozoic and

Paleogene are the main regional unconformities in this area. The Benxi and Taiyuan formations of Carboniferous system and the lower Shihezi formation of Permian system include the gas-prone, coal-measured source rocks, and is the source for coal-formed gas (Lin et al, 2007; Jiang et al, 2010).

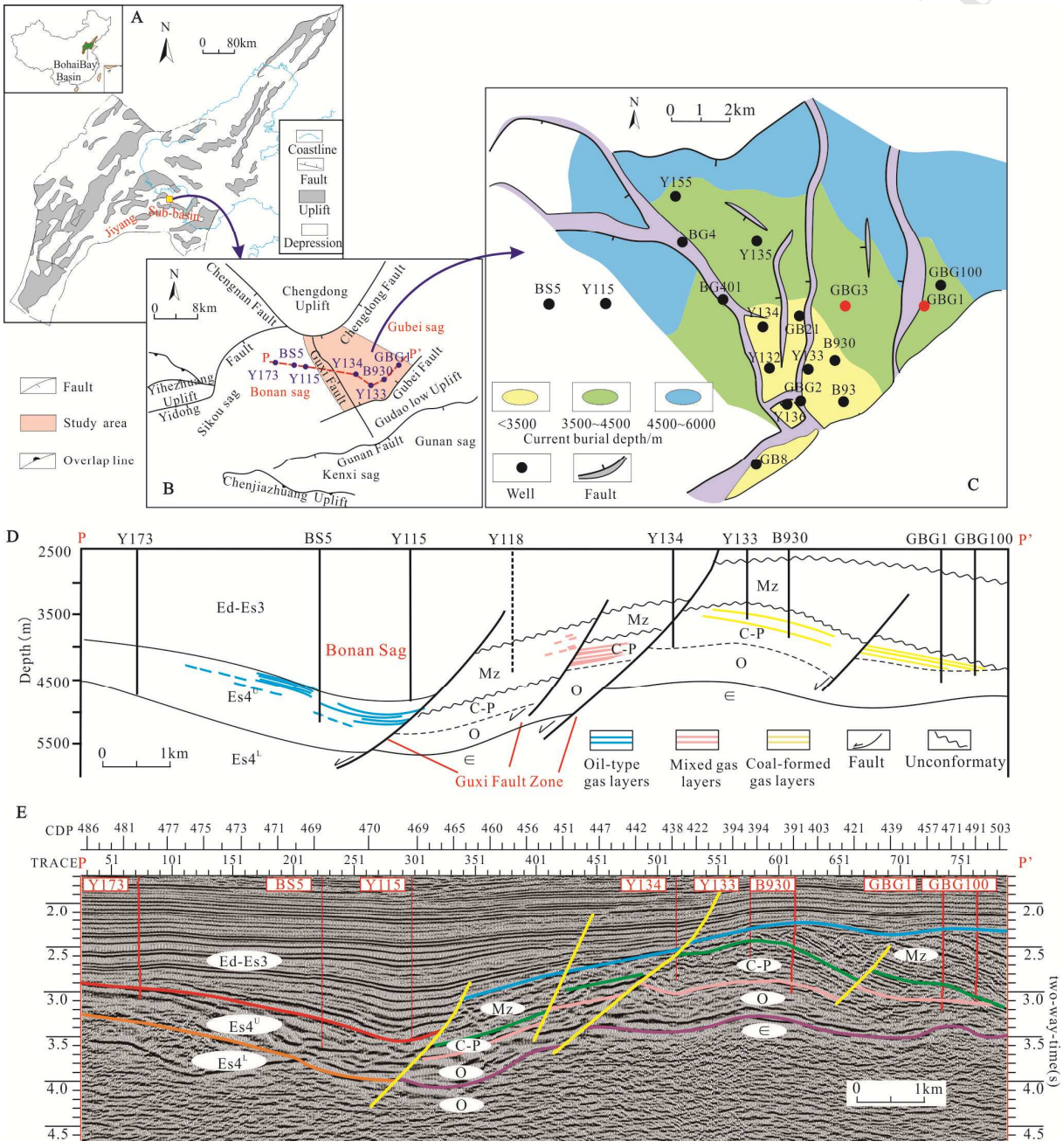

Fig. 1 (A) Location map of Jiyang Sub-basin in Bohai Bay Basin. The point shown by a yellow square with red outline is the location of Gubei area. (B) Map showing the structural location and main boundary

faults of Gubei area. (C) Enlarged detail of the study area showing the burial depth zoning. (D) Cross-section (P-P') of the Gubei gas field showing the various tectonic-structural zones, key stratigraphic intervals and the vertical distribution of natural gas. (The distribution of natural gas was modified from Lin et al, 2007; Jiang et al, 2010). (E) Seismic section of Cross-section (P-P') in Fig1.D

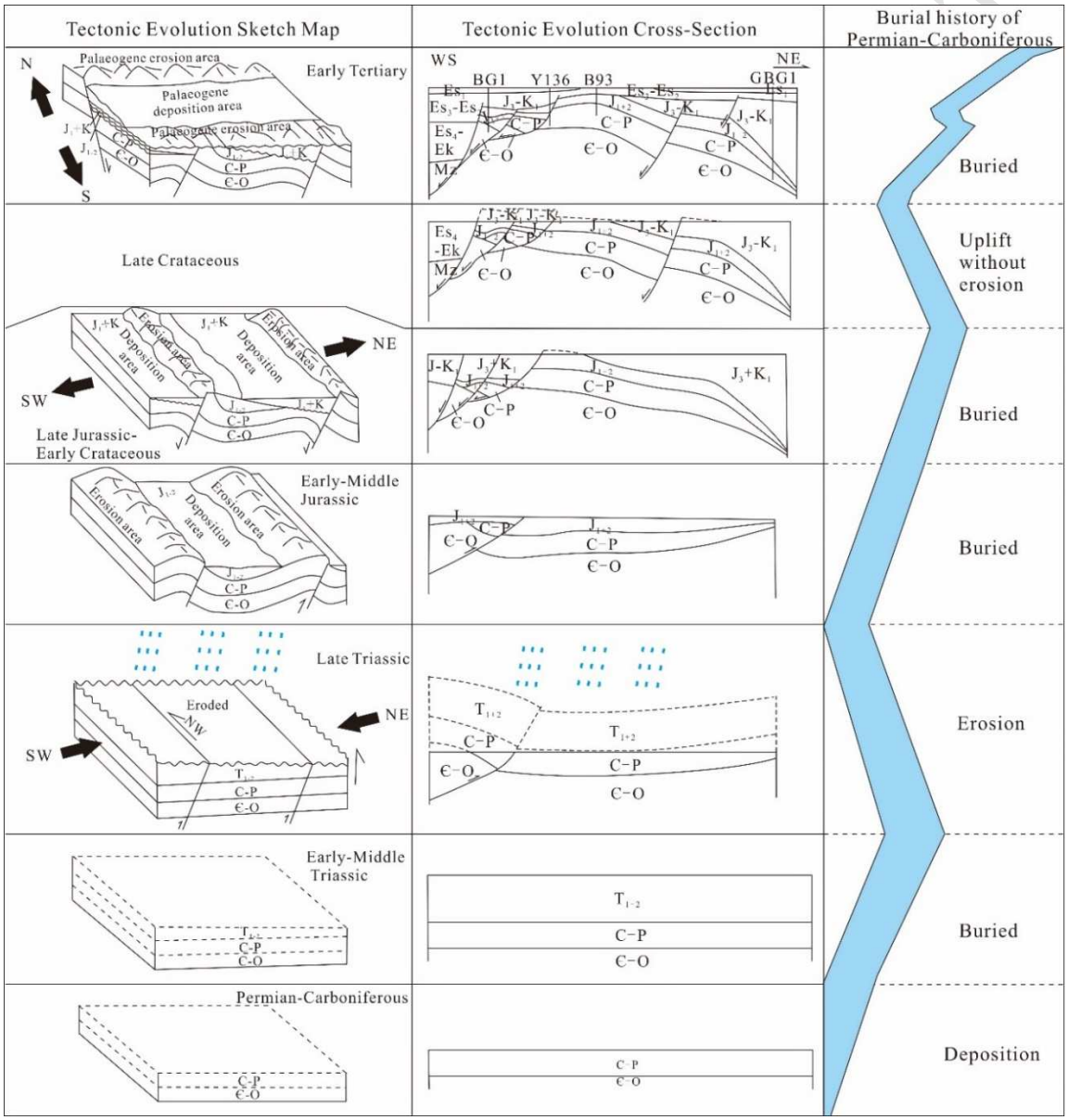

Fig.2 Tectonic evolution shown by sketch map and cross-sections, and its coupling relationship with the burial history of Permo-Carboniferous (Modified from Liu et al., 2007)

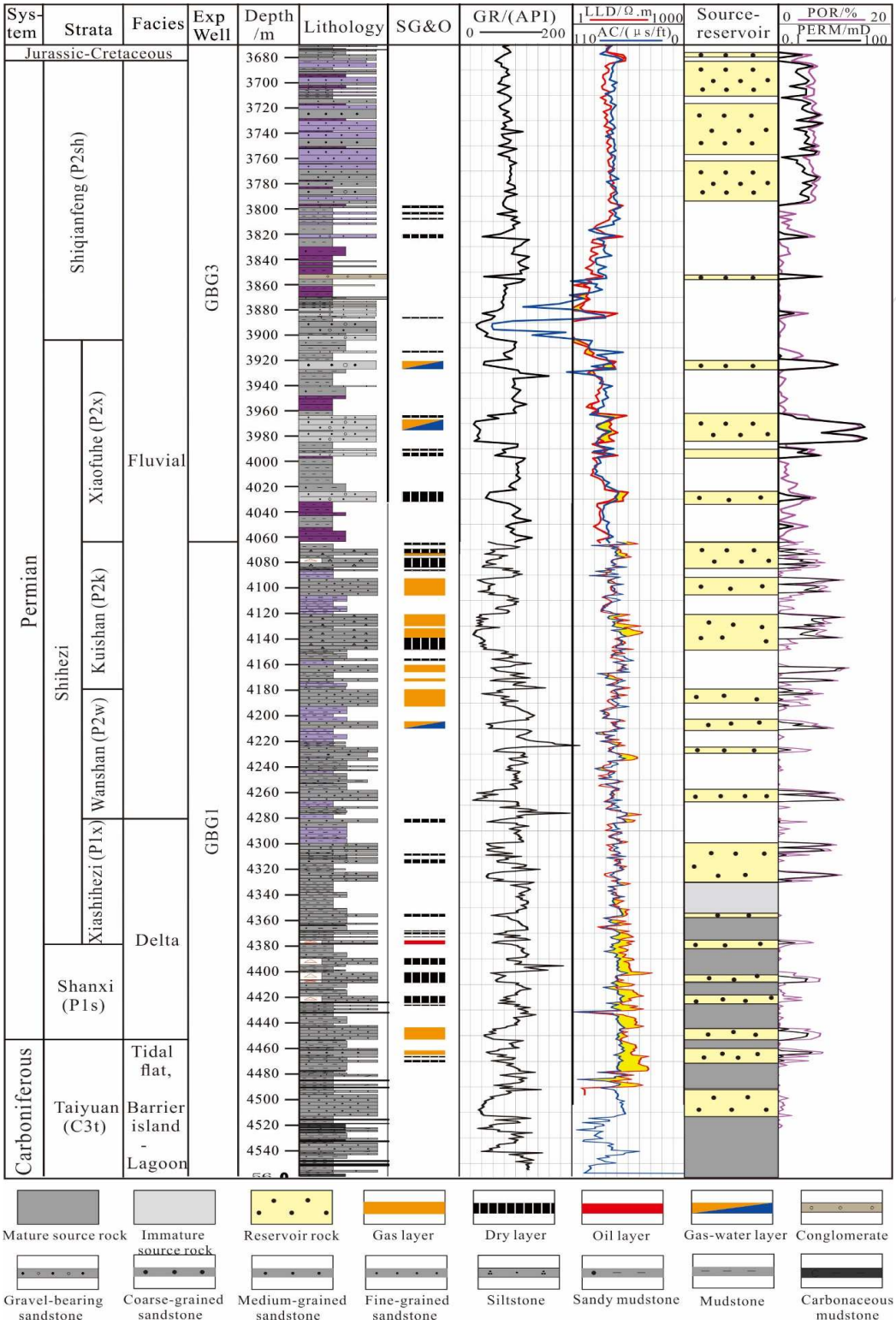

Fig. 3 Permian-Carboniferous stratigraphy of the Gubei gas fields, showing the natural gas-bearing beds and major natural gas system elements (Taken GBG1&GBG3 as example wells, the positions of the wells are shown by red points in Fig.1C). Exp=Example, SG&O=Show of gas and oil. (Modified from Liu et al., 2007)

The Permo-Carboniferous strata were significantly eroded during the Late Triassic

inversion. They now only partially cover the Gubei area. From the central part of the buried hill to the northeast and southwest, the residual strata at the top of Permo-Carboniferous gradually get stratigraphically older. The youngest strata (P_2sh) only remains in small part of the central area (Fig.4).

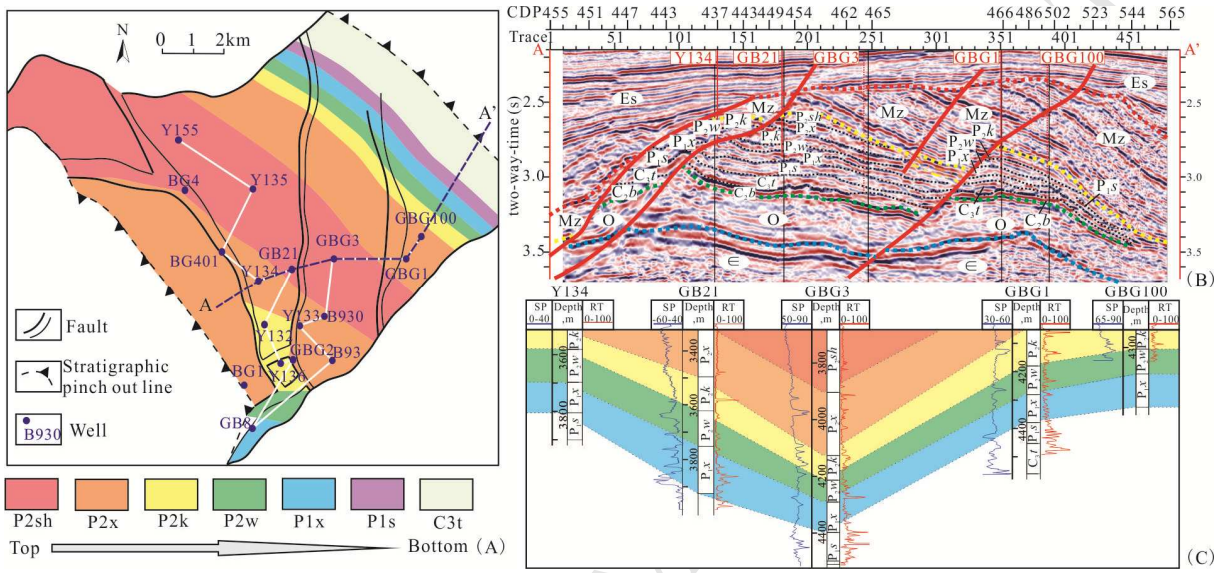

Fig.4 (A) Map showing the residual distribution of different formations of Permo-Carboniferous (Liu et al, 2007); (B)Seismic section and (C) connecting-well profile showing the distribution of the intervals

3. Database and methods

The structure map and seismic sections were provided by the Shengli Oilfield Company of Sinopec China. Basic well data, including well logs and indication of oil and gas of key wells, are used for stratigraphic, lithological and sand body feature analysis.

Rock composition data for 39 thin section samples, 272 measured reservoir porosity and permeability data, as well as 25 groups of bulk rock X-ray diffraction data of whole rock and clay minerals from 4 wells were analyzed. Well locations are shown in Fig.1C.

Thirty-two core samples for thin sections were impregnated with blue epoxy to enable analysis of mineralogy, diagenesis and visual porosity, 32 samples for fluid inclusion thin

sections were prepared as thick doubly polished sections of approximately 100μm thickness, and 20 samples were prepared for cathodoluminescence examination. Thin sections were observed on a Leica DM2500P standard polarizing microscope to identify textures and mineral composition as well as to characterize the relationships between different diagenetic cements and pores. A Leica DFC420C digital camera attached on the microscope was used to take photomicrographs, and point counting device was used to quantitatively estimate the percentage of different rock components such as detrital grains, cements and matrix.

Representative samples were selected for Hitachi TM1000 tabletop scanning electron microscope (SEM) observation and energy-dispersive x-ray spectroscopy (EDS) detection to assign the mineral compositions. The petrographic examination of fluid inclusion thin sections was carried out based on Zeiss AXIO Imager D1m digital polarized fluorescence microscope, and the micro-thermometry of aqueous inclusions was conducted using a calibrated Linkam. THMS600 gas-flow heating/freezing system. The homogenization temperatures (Th) were obtained by cycling. Th measurements were determined using a heating rate of 10 ℃/min when the temperature was lower than 70℃ and a rate of 5℃/min when the temperature exceeded 70°C. The measured temperature precision for Th is ±1°C. Burial and thermal history were analyzed by 1D module of the Schlumberger software PetroMod (V2012.1) based on data from exploration wells.

4. Results

4.1 Sand body features and the occurrence of natural gas

Based on the basic geological data from exploration wells, statistics for the net to gross ratio suggest that sand body features vary in different members of Permo-Carboniferous. The

ratio of P_2k is the largest, ranging from 50.40% to 73.81% with an average of 59.43%, followed by P_2w, P_1x, P_1s and C_3t with an average ratio of 43.24%, 42.56%, 42.02%, 38.97% respectively. The P_2x has the smallest ratio from 11.75% to 49.06% with an average of 30.11% (Fig.5). From updip wells to the wells located downward, the figures of P_2k and P_2w remain stable, while those of other members fluctuate greatly (Fig.5), revealing that the continuity and lateral extent of sand bodies in these two members are the best.

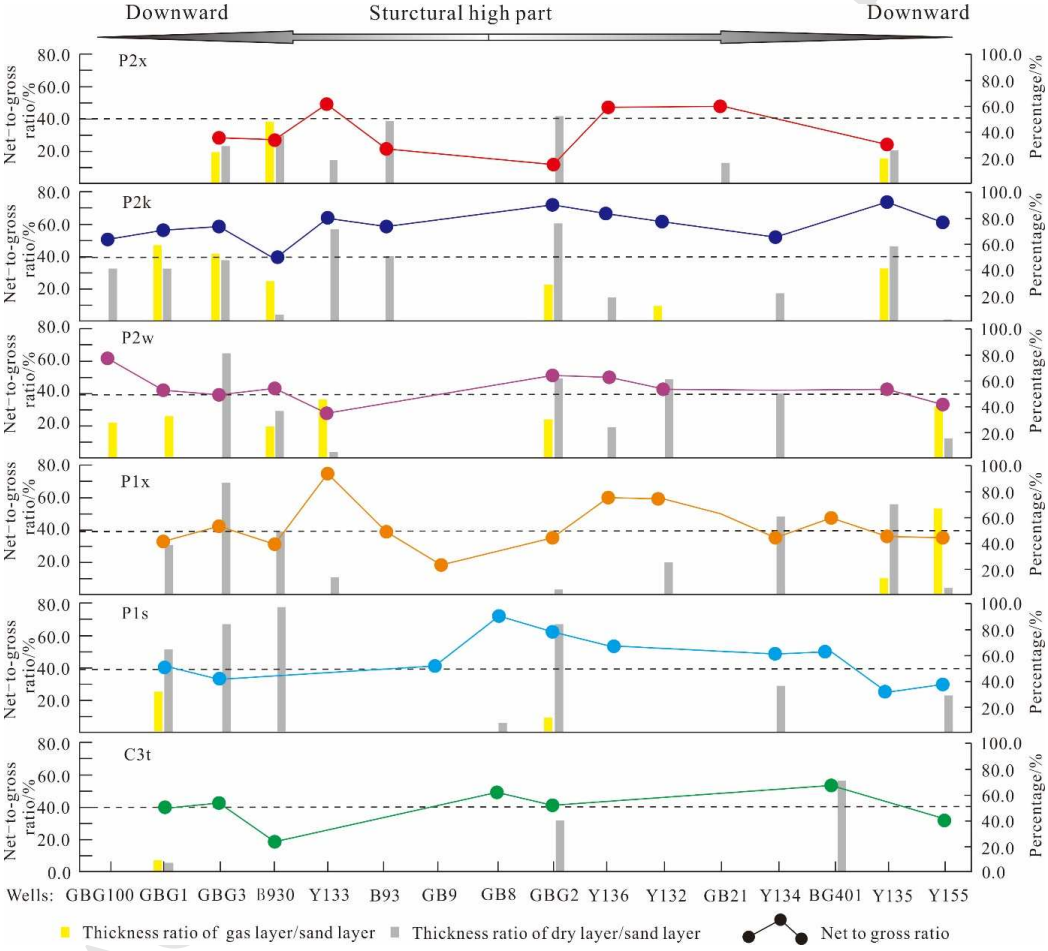

Fig.5 Charts showing the net to gross ratios of different members in Permo-Carboniferous, distribution of natural gas layers and the correlation between them. The horizontal variation was demonstrated by the values of well sites along the structural trends. The cross-well line was shown by white line in Fig.4.

The thickness ratio of gas layers to sand layers of every single formation was calculated. As shown in Fig.5, the natural gas mainly accumulated in the P_2k and P_2w members of Permian

where net to gross ratio are relatively high and uniform.

With regard to single sandstone beds, all the stratigraphic members of the Permian system are dominated by thin sandstone beds with thickness less than 2 m (accounting for over 40% of the total layers) (Fig.6A&B). The proportion of sandstone beds thinner than 2 m in P_2k is the smallest (48%), followed by the P_2w and P_1s (approximately 60%). The P_2x and P_1x have the largest proportion of thin beds (around 70%) (Fig.6B). However, all the natural gas accumulations occur in the sandstone beds with thicknesses over 1.9m. In other words, the minimum thickness of gas-bearing beds is 1.9 m (Fig.6C).

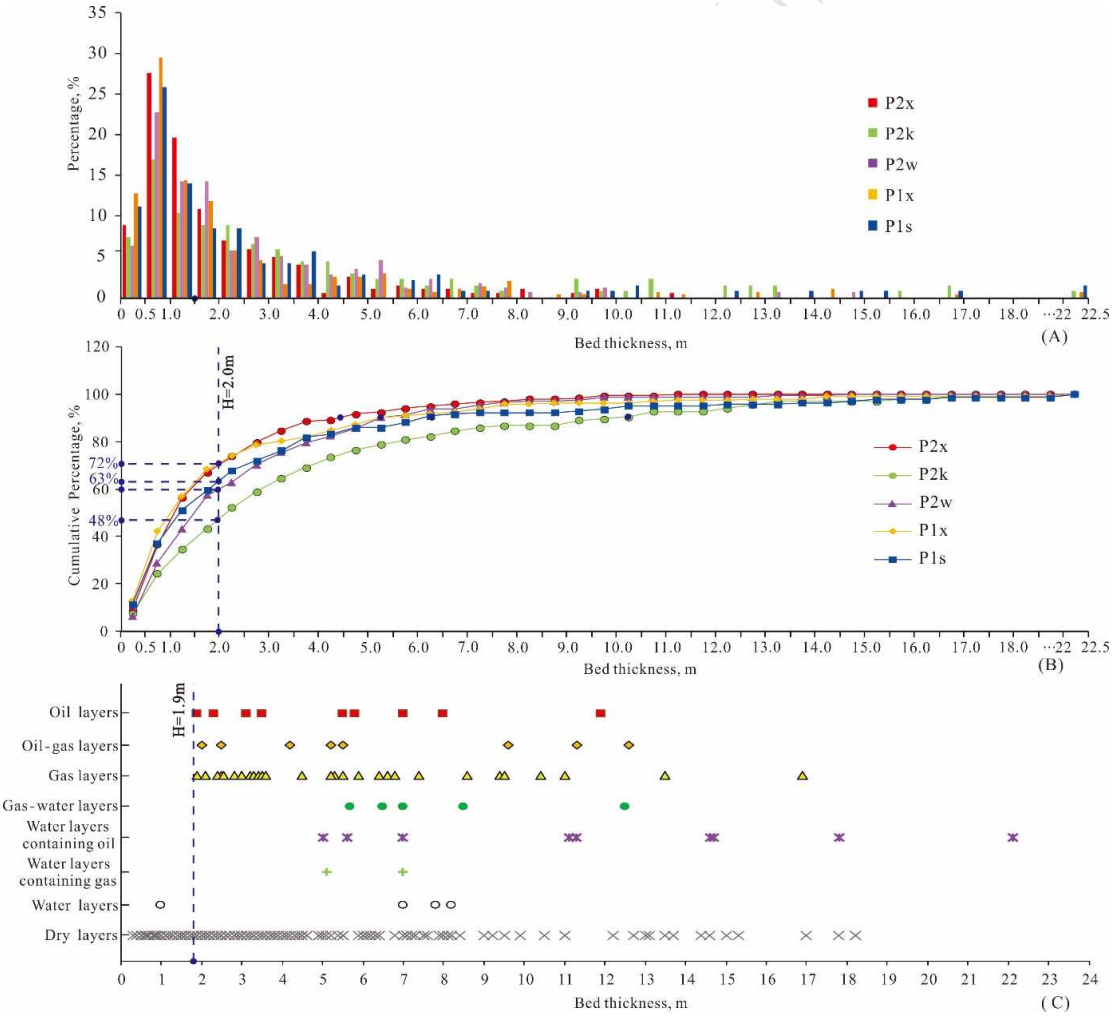

Fig. 6 (A) Bar chart showing bed thickness distribution of different members in Permo-Carboniferous; (B) Cumulative frequency line chart of chart A; (C) Diagram showing thickness of hydrocarbon-bearing

sandstone beds

4.2 Porosity and permeability

The Permian sandstones have a wide range of porosity from 0.23% to 28.08% (Fig.7A). In general, the porosity decreases as the burial depth increases from 2500m to 4500m, but an anomalously high porosity exists in the depth intervals from 3500m to 4500m (Fig.7A). The Permian reservoir rocks are dominated by sandstones with porosity less than 10% porosity (over 90%) (Fig.7 B&C). With regard to the gas-bearing beds, the porosity varies from 1.5% to 17% (mainly in the range of 4%-10%), the permeability ranges from 0.08 mD to 785.97 mD (dominated by 0.1-1mD) (Fig.7 D&E).

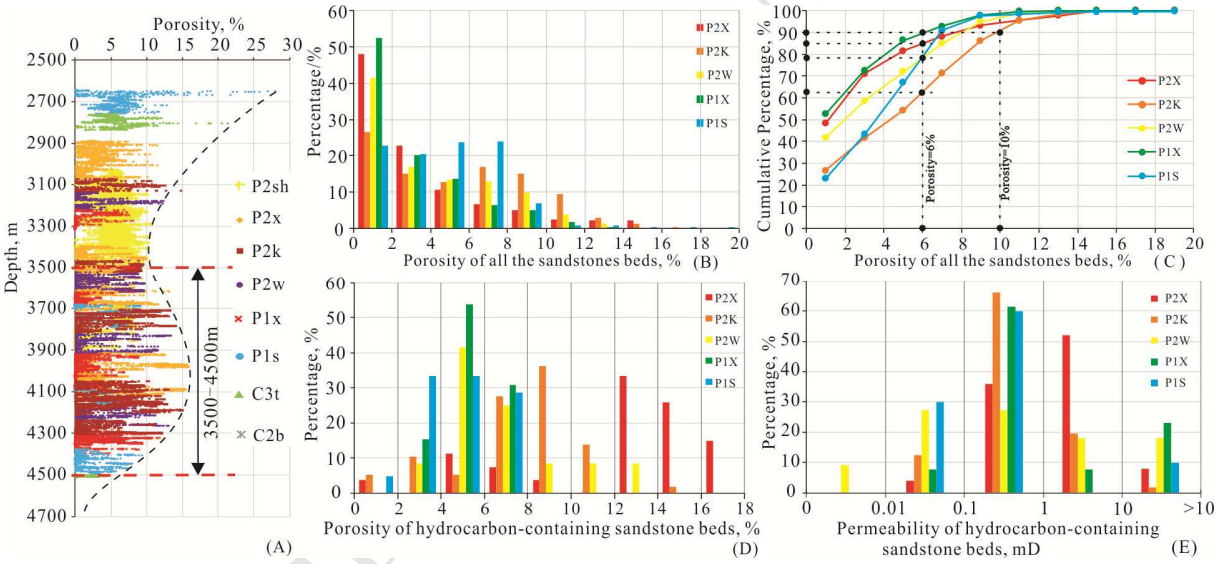

Fig.7 A: Plots showing porosity variation versus depth (well-logging interpretation data); B-C: Chart showing the porosity of different formations (well-logging interpretation data); D-E: Chart showing the porosity and permeability of hydrocarbon-containing sandstone beds (measured data).

With regard to the relationship between the bed thickness and the maximum porosity of every single bed, all members of Permian show a similar pattern: for beds thinner than about 2.0m, the maximum porosity of single bed has a positive correlation with the bed thickness, ranging from 0.31% to 17.88%; while for thicker beds, the porosity remains uniform (Fig.8A).

In order to further understanding the essential cause of this feature, the porosity variation within every sandstone bed was analyzed. For the sandstones with distance to the top sandstone/mudstone interface less than 1.25 m and the sandstones with distance to the bottom sandstone/mudstone interface less than 0.75 m, the porosity varies greatly, and there is a positive correlation between the distance and porosity (Fig.8B). However, the sandstones with distance to top interface over 1.25 m and to the bottom over 0.75m have a uniform porosity from 4% to 12% (Fig.8B). This indicates that there is a porosity transitional zone at the top and bottom of every single bed, the porosity transitional zone of the bottom with thickness of 0.75 m is much thinner than that of the top with thickness of 1.25m (Fig. 8C). The total thickness of the top porosity transitional zone (1.25m) and the bottom transitional zone (0.75m) is 2m. It can be found that this value perfectly matches the threshold value of porosity in Fig.8A. This illustrates that the porosity variation versus sandstone bed thickness shown in Fig.8A perhaps relate to the existence of the porosity transitional zones in every single bed. Besides, as is shown in Fig.6C, the gas-bearing sandstone beds are all thicker than 1.9m, which is very close to the threshold value of porosity in Fig.8A (2m). This indicates that the differential filling of natural gas in sandstones may be related to the existence of the porosity transitional zones in every single bed as well.

It is worth to note that “the marginal sandstones” in the paper refer to the sandstones with distance to the top sandstone/mudstone interface less than 1.25 m and the ones to the bottom sandstone/mudstone interface less than 0.75 m, and the “the central sandstones” in the paper refer to the sandstones between the top and the bottom marginal sandstone zone. The details of sandstone samples analyzed in the paper are listed in Table.1.

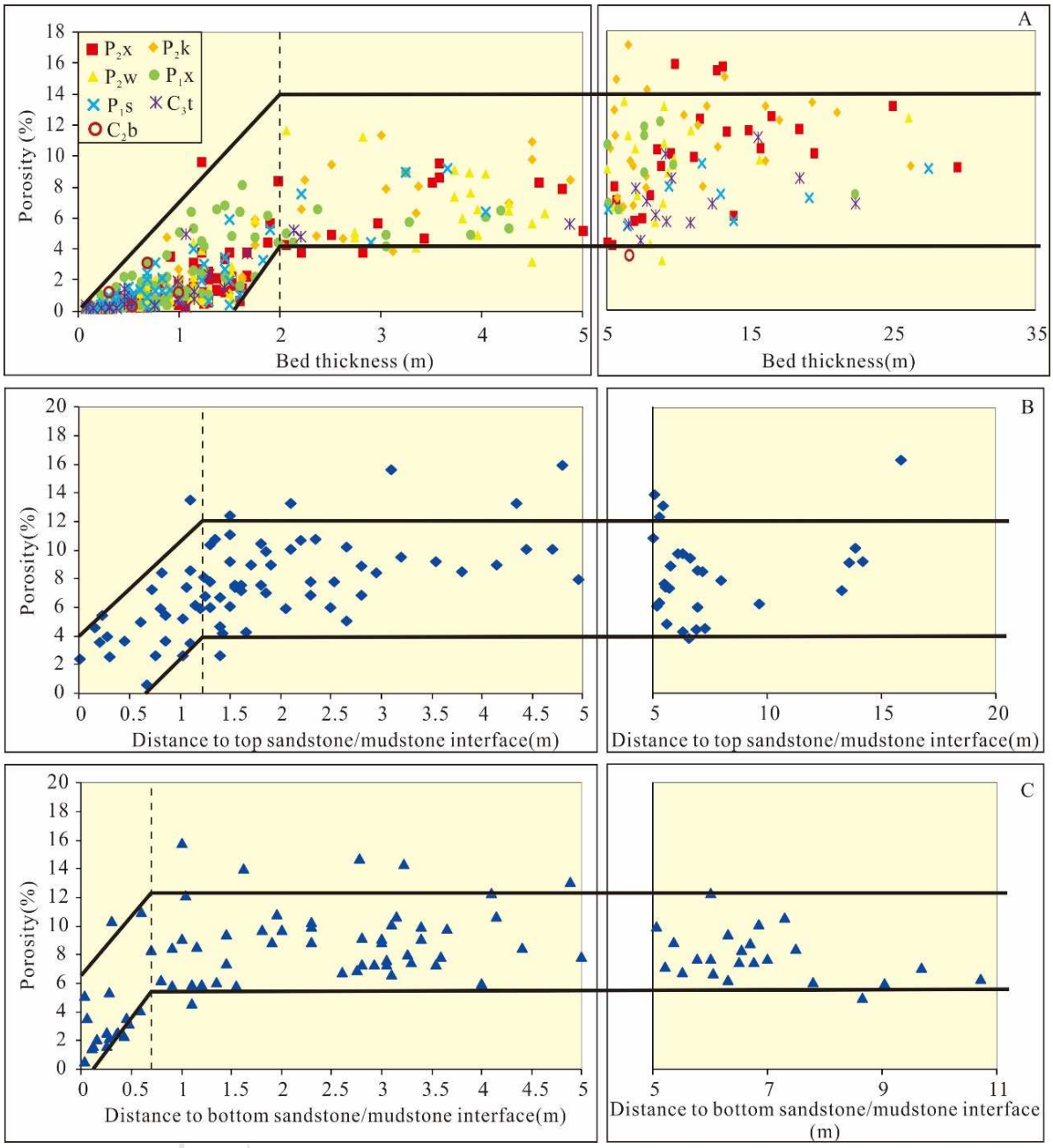

Fig.8 Plot showing porosity variation with (A) Bed thickness of different members in Permo-Carboniferous, (B) Distance to top sandstone/mudstone interface, and (C) Distance to bottom sandstone/mudstone interface

Table.1 The information of sandstone samples analyzed in the paper

Wells	Formation	Depth,m	Top depth of the bed, m	Bottom depth of the bed, m	Distance to the top contact, m	Distance to the bottom contact, m	Sample classification
B930	P_2x	3621.30	3619.88	3627.12	1.42	5.82	Central
B930	P_2x	3622.61	3619.88	3627.12	2.73	4.51	Central
B930	P_2x	3669.03	3668.04	3677.64	0.99	8.61	Marginal
B930	P_2x	3671.25	3668.04	3677.64	3.21	6.39	Central
B930	P_2x	3673.50	3668.04	3677.64	5.46	4.14	Central
B930	P_2x	3675.10	3668.04	3677.64	7.06	2.54	Central
GBG1	P_2k	4075.15	4074.65	4075.25	0.50	0.10	Marginal
GBG1	P_2k	4076.65	4076.03	4081.25	0.62	4.60	Marginal
GBG1	P_2k	4077.85	4076.03	4081.25	1.82	3.40	Central
GBG1	P_1s	4401.54	4400.50	4409.50	1.04	7.96	Marginal
GBG1	P_1s	4402.30	4400.50	4409.50	1.80	7.20	Central
GBG2	P_2k	3519.30	3498.65	3524.86	20.65	5.56	Central
GBG2	P_2k	3523.00	3498.65	3524.86	24.35	1.86	Central
GBG2	P_2k	3547.85	3545.74	3550.77	2.11	2.92	Central
GBG2	P_1x	3690.80	3690.60	3691.10	0.20	0.30	Marginal
GBG3	P_2x	4086.20	4081.65	4099.03	4.55	12.83	Central
GBG3	P_2k	4161.80	4148.63	4165.63	13.17	3.83	Central
Y132	P_1x	3598.20	3596.50	3604.00	1.70	5.80	Central
Y132	P_1x	3599.20	3596.50	3604.00	2.70	4.80	Central
Y132	P_1x	3600.60	3596.50	3604.00	4.10	3.40	Central
Y133	P_2x	3281.30	3279.69	3281.64	1.61	0.34	Marginal
Y133	P_2x	3325.27	3325.11	3325.91	0.16	0.64	Marginal
Y135	P_2sh	4161.28	4160.43	4161.28	0.85	0.00	Marginal
Y135	P_2sh	4164.00	4163.65	4164.95	0.35	0.95	Marginal
Y135	P_2sh	4333.76	4333.00	4333.81	0.76	0.05	Marginal
Y136	P_2w	3701.25	3700.00	3703.62	1.25	2.37	Marginal
Y136	P_1x	3706.00	3705.00	3705.20	1.00	0.20	Marginal

4.3 Sandstone petrology: detrital mineralogy

The studied Permian sandstones are fine to coarse-grained with grain sizes ranging from 0.06 mm to 2 mm and shown as texturally immature. The detrital grains are mostly sub-angular and sub-rounded, and poor- to moderate-sorted (Fig.9). As for the clastic compositions, the sandstones are mostly sublitharenites, feldspathic litharenites, litharenites according to Folk (1980), demonstrating as compositionally immature with an average framework composition of $Q_{51}F_{10}L_{39}$ (Fig.10A). There is no obvious difference in petrologic

composition between different stratigraphic members. However, the petrologic composition of the marginal sandstones and the central sandstones is quite different. The central sandstones have a more mature composition ($Q_{62}F_5R_{33}$) than the marginal sandstones ($Q_{37}F_{17}R_{46}$) (Fig.10B). The proportion of feldspar and rock fragment increases linearly with the decrease of feldspar and rock fragment secondary porosity (Fig.10C). The central sandstones have more feldspars and rock fragments dissolution pores but less remained feldspars and rock fragments than the marginal sandstones (Fig.10C). The negative linear relationship between the two illustrates that the initial composition of them might be similar, and the mineral dissolution probably account for the difference between the marginal sandstones and the central sandstones on the total content of feldspar and rock fragment.

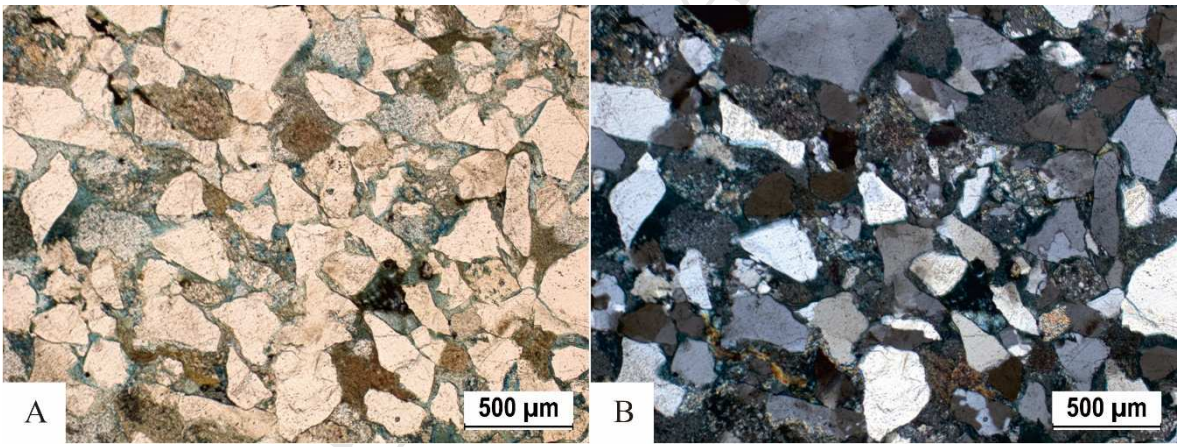

Fig.9 Photomicrographs in the (A) polarized light view and (B)cross-polarized light view, showing the sandstone textural and compositional characteristics of sandstones. Taken the sample of GBG3 (4161.80m) as example.

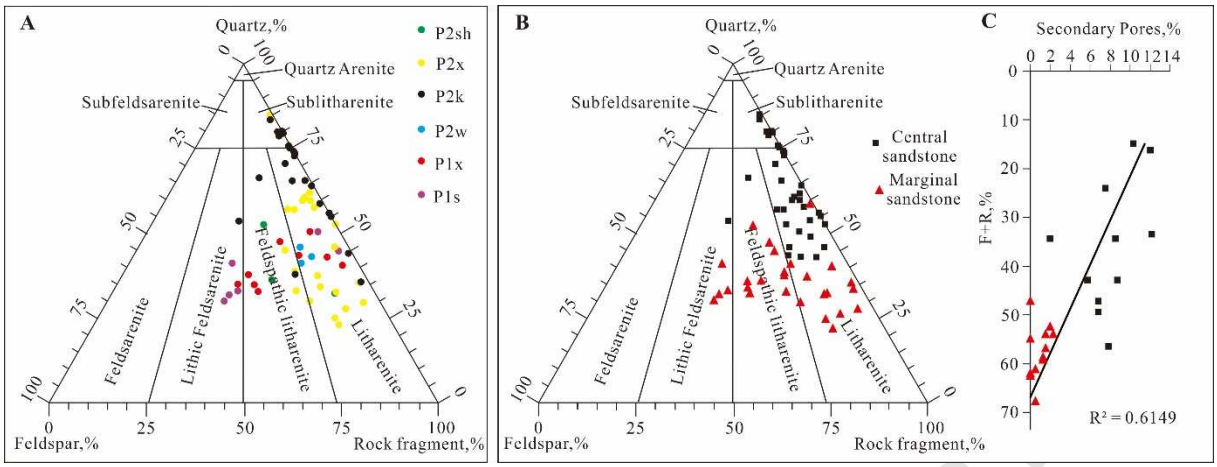

Fig.10 Rock composition of (A) the different members in Permian sandstones in the Gubei area; (B) central sandstones and marginal sandstones; (C) plot showing the correlation between secondary pores and the total content of feldspar and rock fragment. (Ternary plot refers to sandstone classification standard of Folk et al. (1970))

4.4 Sandstone diagenesis

The intergranular contacts vary from long to concavo-convex contacts (Fig.11A), and many easily deformable grains were heavily deformed and fill the primary intergranular porosity, to the point where it could be classed as pseudomatrix or could be mistaken for detrital clay and silt (at black arrow in Fig.11 B and white arrow in Fig.11C). The features indicate that the sandstones experienced strong compaction. Residual primary pores are rarely remained in the sandstones (Fig.11). Almost all the pores are secondary pores caused by grain dissolution of feldspars, and rock fragments (Fig.11). The marginal sandstones tend to have no or only a few dissolution pores with porosity from 0.3 % to 4.5%, but the central sandstones have much more dissolution pores than marginal sandstones (about 3.8 % to 12.0 %). This illustrates that the intensity of mineral dissolution in central sandstones is stronger than marginal sandstones. Accordingly, the feldspars and rock fragments mostly occur as fresh grains in the marginal sandstones (Fig.11D), while they commonly occur as partially dissolved grains in the central

sandstones (Fig.11J-O).

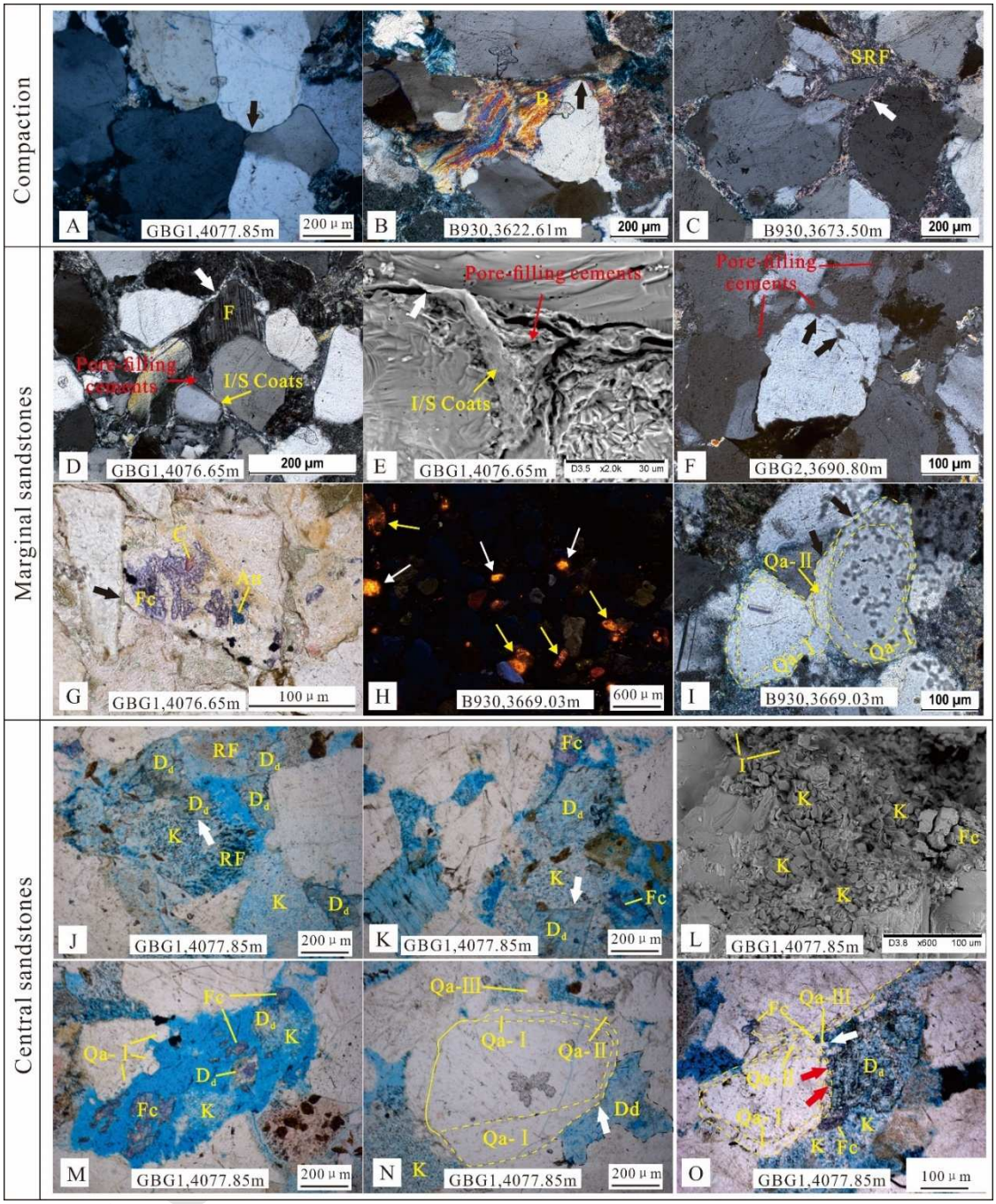

Fig.11 A-C Images of sandstones showing compaction: A, Long to concavo-convex contacts between quartz grains; B, Squeezed biotite; C, Sedimentary rock fragment squeezed into pore space shown as pseudomatrix. D-I Images of marginal sandstones: D, Grain-coating clays and pore-filling cements in the cross-polarized light view (XPL); E, SEM image of grain-coating clays and pore-filling cements; F&I, Quartz overgrowth in XPL; G, Carbonate cements presenting as replacement of detrital grain; H, CL

image of carbonate cements. J-O Images of central sandstones (pore space is shown in blue): J,K,M,N-O, Thin section images showing paragenesis of diagenetic events in polarized light; L, SEM image of authigenic kaolinite in dissolution pores. B=Biotite, SRF=Sedimentary rock fragment, F=Feldspar, I/S=Illite/smectite mixed layer, C=calcite, Fc=Ferrocalcite, An= Ankerite, Qa=Quartz overgrowth, K=Kaolinite, D_d=Dissolved dolomite, RF=Rock fragment, I=Illite. The information of the samples is shown in Table.1.

The authigenic minerals in the marginal sandstones and the central sandstones are roughly the same and include quartz cements, carbonate cements, authigenic clay minerals, and a small amount of iron cements. Among them, quartz cements and authigenic clays are the two most common types of diagenetic minerals, representing 1%-8.5% and 3%-25% of the whole rock, respectively (Fig.12 D-E), while carbonate cements are less important with a proportion of no more than 3% (Fig.12 C). Ferrocalcite and dolomite are the most common carbonates (Fig.12 C). Four types of clay minerals, kaolinite, illite, I/S and chlorite were observed as well, among them kaolinite made up the largest proportion (about 50%) (Fig.12 A-B). However, the result of diagenetic mineralogy examination indicates that the marginal and the central sandstones have experienced different diagenetic processes (Fig.11) and the content of the cements shows obvious difference (Fig.12D-E).

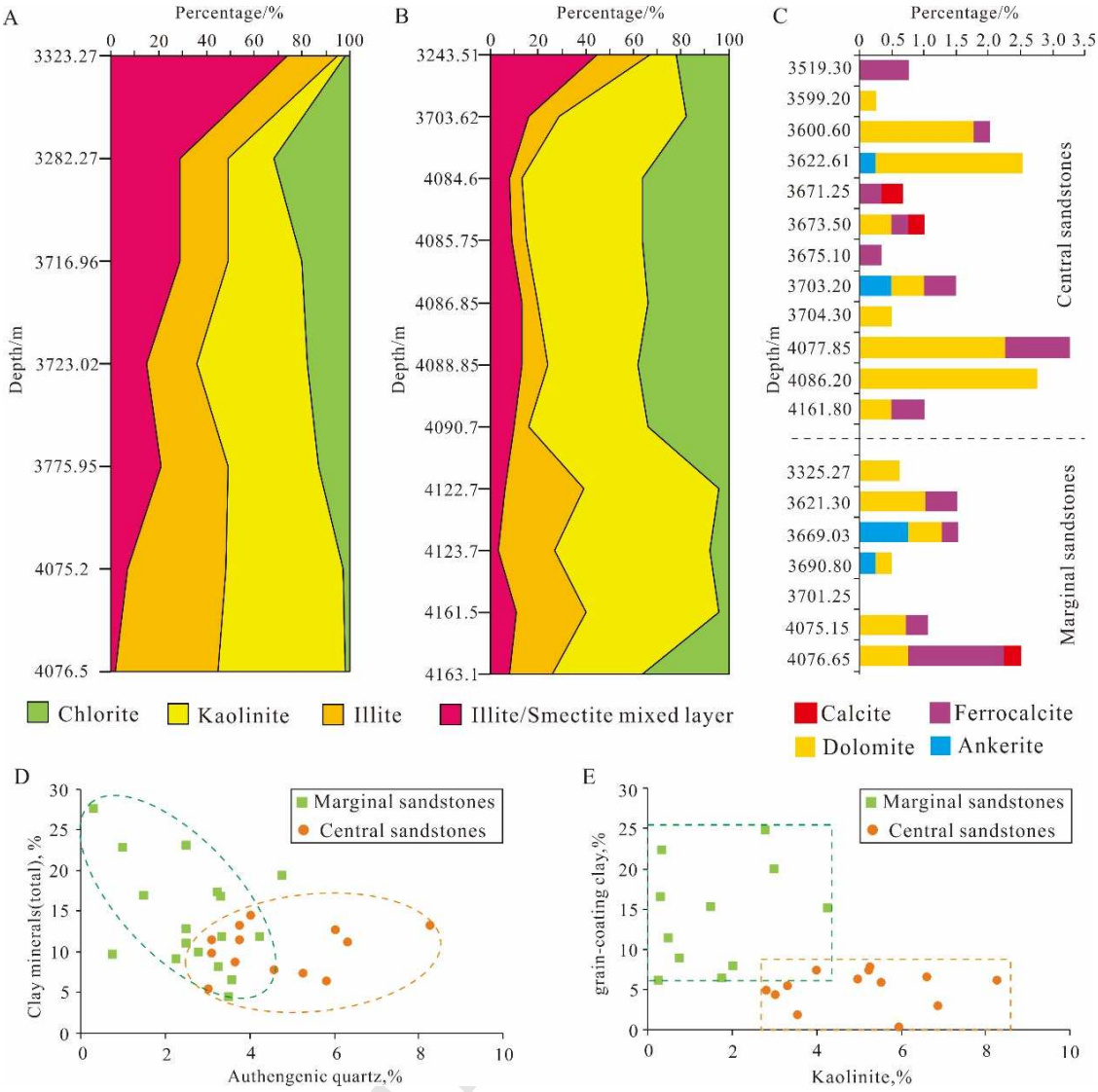

Fig.12 Charts showing content of authigenic minerals in Permian sandstones, Gubei area. (A) clay cements composition in marginal sandstones; (B) clay cements composition in central sandstones; (C) carbonate cements; (D) plot showing the correlation between authigenic quartz and clay minerals; (E) plot showing the correlation between authigenic kaolinite and grain-coating clay. The information of the samples is shown in Table.1.

For marginal sandstones, most of the grains are coated by clay minerals with moderately high birefringence and light brown to green color, which are mostly recognized as I/S mixed layers by SEM-EDS examination (Fig.11 D-E, G). The clays may have precipitated or infiltrated prior to the principal period of compaction because the clay coating continues

around the grains even at grain-to-grain contacts (white arrow in Fig.11D-E). Such grain-coating cements can be quite effective in isolating the framework grains from pore waters and thus in inhibiting later formation of overgrowth cements on quartz, feldspar and other detrital grains (Ajdukiewicz and Larese, 2012). After the grain-coating clay cements, the chalcedony-like cements with low first-order birefringence (to anomalous) colors filled (Ulmer-Scholle et al., 2014) and completely obliterate the remaining primary porosity (the part marked as pore-filling cements in Fig.11D, F). Although the marginal sandstones are usually supported by grains with long contacts, some of the grains partially "floated" or isolated by thin pore-filling cements illustrating the cements precipitated or infiltrated at the early stage of diagenesis with little compaction as well. The carbonate cements in marginal sandstones, dominated by highly ferroan calcite (stained deep purple to blue), were mostly precipitated as intragranular mineral replacements of feldspars and rock fragments, and commonly occur as microsparry or sparry interlocking mosaic of crystals with the crystal size varies from 4 mm to 200 mm (Fig.11 G-H). This indicates the limitation of spaces during crystallization. Only a few quartz cements occur in marginal sandstones, which probably due to the inhibition of grain-coating clays. Quartz cement is present mainly as overgrowths, and two stages of overgrowth were identified based on the impurity lines or dust rims outlining the original surfaces of the detrital grain. The first stage of overgrowth with thickness ranging from 15μm to 80μm, commonly presents as coats around euhedral quartz grains, while the stage-□ occurs mainly as primary pore-filling shape partially attaching on the grains or stage-I overgrowth (Fig.11 I). The overgrowths tend to grow at the sites where the clay coats are thin or lacking, and it can be clearly seen that the grain-coating clays are partially enclosed

by the quartz overgrowths (black arrows in Fig.11 F). This indicates that the quartz overgrowths postdated the clay coatings. The overgrowth exists at the grain-contact points (black arrows in Fig.11 I), which means that the cementation occurred before the grains are compacted to be contacted with each other, in other words, the cementation occurred in the early diagenetic stage with less compaction.

The clay coats and intergranular cements are absent or much less present in central sandstones than in marginal sandstones (Fig.11A, Fig.12D-E). The authigenic clays are dominated by kaolinite that commonly occurs as euhedral booklets and vermicular aggregates in dissolution pores (Fig.11 J-O). Two forms of carbonate cements can be identified: one is partially dissolved dolomite, the other is ferrous carbonate cement precipitated in the dissolution pores (Fig.11 J-K, M, O). The dolomite precipitated after the kaolinite and occupied part of kaolinite space, but was dissolved during subsequent diagenesis process. The latter ones were mainly precipitated in dissolution pores (including the dolomite dissolution pores) or as the replacement of early-formed dolomites (Fig.11M), presenting as sparry crystals (50-200 mm) and clusters with no obvious signs of dissolution. This illustrates that the precipitation of carbonate cements postdated the dissolution of early-formed dolomites. Quartz cements occur in central sandstones in two forms: quartz overgrowth and the small authigenic quartz crystals in the dissolution pores. Three stages of quartz overgrowths were identified according to the optical discontinuity, impurity lines or dust rims outlining the original surfaces of the detrital grain, or the presence of inclusion clouds and vacuoles within the quartz grain. The compromise outline of early-formed dolomites at the contact with stage-I overgrowth (white arrow in Fig.11N) indicates that dolomite precipitated after the

stage-I overgrowth. The dolomites were partially enclosed in stage-□ overgrowth (red arrows in Fig.11O), revealing that the stage-□ overgrowth postdated the dolomite. While some ferrocalcite crystals were found to be enclosed in stage-□ overgrowth (white arrow in Fig.11O) illustrating that the stage-□ overgrowths were later-formed.

4.5 Fluid inclusions

Aqueous inclusions can provide important information on temperature, pressure and fluid composition during the precipitation of diagenetic minerals (Robinson and Gluyas, 1992). The aqueous fluid inclusions in samples were mainly wrapped along the healed grain-sized fractures in quartz grains (Fig. 13B), as well as some occur in quartz overgrowths (Fig.13A-B). At room temperature, the inclusions are primarily two-phase inclusions with gas bubbles. The diameter of inclusions are about 1μm – 8μm, and the gas liquid ratio ranges from 3% to 20%.

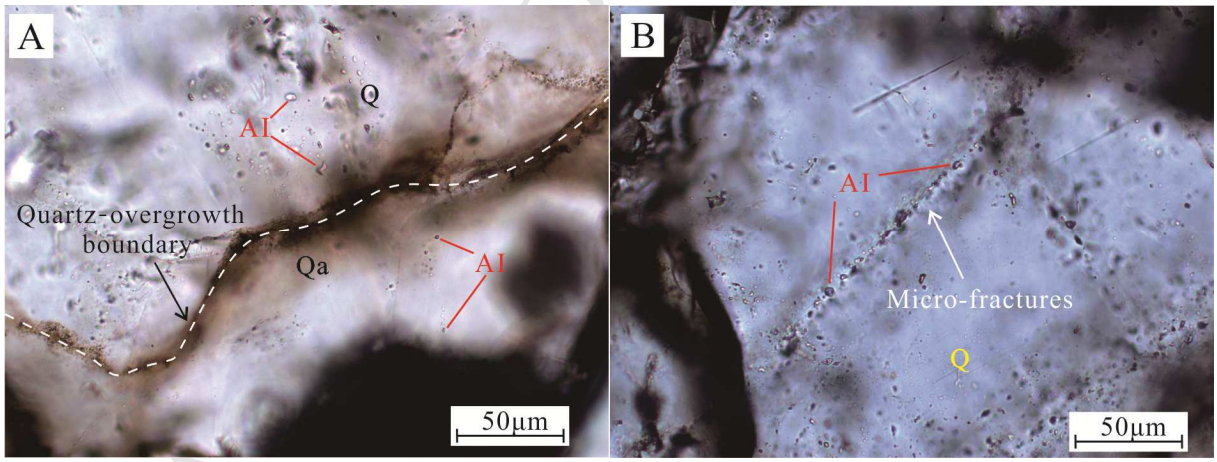

Fig.13 Photomicrographs of aqueous inclusions under transmitted light observed at room temperature in Permian sandstones samples from Gubei area. (A) Aqueous inclusions in quartz overgrowths. (B) Aqueous inclusions along healed microfractures in quartz grains and in quartz overgrowths. AI-Aqueous fluid inclusions, Q-Quartz grains, Qa-Quartz overgrowths.

The distribution of the measured homogenization temperatures (T_h) of the aqueous

inclusions were presented in Fig.14A-B. The T_h of aqueous inclusions in healed micro-fractures and quartz overgrowth in central sandstones is basically identical, mainly distributed in three intervals, ranging from 60°C to 80°C, 105°C to 125°C and 135°C to 155°C respectively (Fig.14 A). This suggests that one stage of quartz cementation occurred in eodiagenetic and two occurred in mesodiagenetic stages individually, which is in consistent with thin section observation (Fig.11O). There are only two T_h intervals of aqueous inclusions in quartz cements in marginal sandstones, from 65°C to 90°C, 95°C to 130°C respectively (Fig.14 B), indicating one stage of quartz cementation in eodiagenetic and one in mesodiagenetic stage. This also coincides with the thin section observation.

T_h of two-phase aqueous inclusions in carbonate cements of central sandstones ranges from 65°C to 95°C and 100°C to 130°C respectively (Fig. 14C), revealing that two stages of carbonate cementation occurred in the sandstones. It is also corresponding perfectly with the petrography texture relationship (Fig.11M). The aqueous inclusions in carbonate cements in marginal sandstones ranges mainly from 75°C to 90°C and 105°C to 115°C respectively (Fig. 14 D), which suggests two stages of carbonate cementation as well.

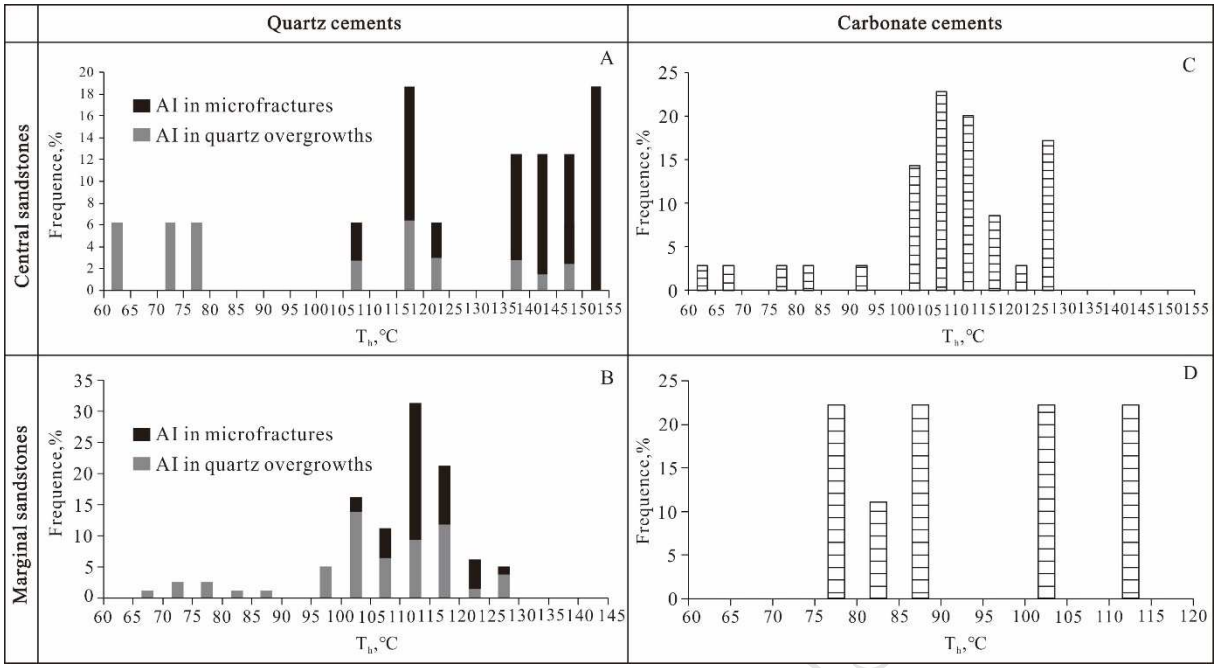

Figure 14. Histograms of homogenization temperature (Th) for aqueous inclusions in healed microfractures of quartz grains, quartz overgrowths and carbonate cements from the Permian sandstones in the Gubei Gas field, Jiyang Depression. AI: Aqueous inclusions.

5. Discussion

5.1 Acids for mineral dissolution

In previous studies, meteoric water, organic acids, and carbonic acid are regarded as the major causes of mineral dissolution (Krynine,1949; Yu et al, 2018; Surdam et al, 1975,1984 and 1989; Kharaka et al, 1985). Among them, organic acids make the key contribution for the secondary porosity, and type-□ kerogen is the best raw material for organic acid production (Crossey, 1984). The concentration of organic acids reaches the peak at 80-120°C in the thermal evolution profile of organic matter (Surdam,1989) and decreases dramatically in the temperature range of 120-200°C because of the thermal decarboxylation to carbon dioxide. In the study area, coal-measured source rocks, mainly composed of type-□ organic matters, are developed in lower Permo-Carboniferous with total thickness ranging from 0 to 250 m. The

Ro of organic matter in the source rocks ranges from 0.98 % to 1.77 % (Fig.15). The temperature reaches 80 °C for the first time in the Early Cretaceous (approximately 115 Ma) and rose to the maximum temperature of 135 °C in the Middle Cretaceous (around 100 Ma) before the uplift movement in the Late Cretaceous. The period from the Early to the Middle Cretaceous was the main period of organic acid generation. Subsequently, a large amount of CO_2 was released in the temperature range of 120-200 °C (corresponding to the duration of Neogene to date) due to the thermal decarboxylation of organic acids.

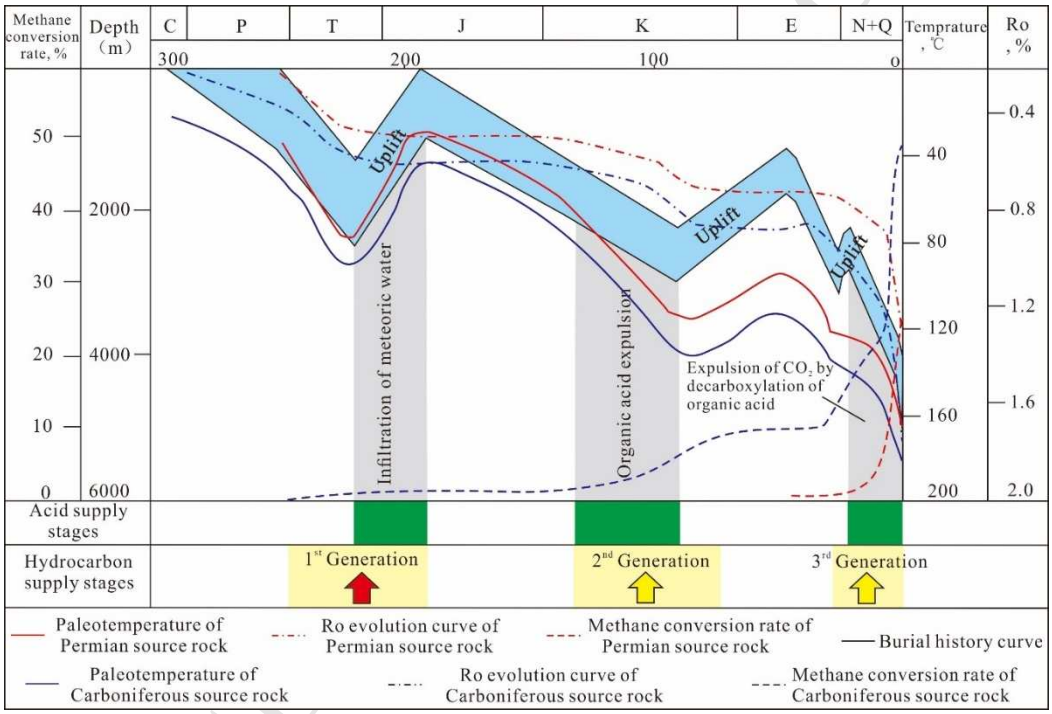

Fig.15 Determination of acid supply stages by comprehensive analysis of the burial, thermal and hydrocarbon generation history of Permo-Carboniferous in Gubei area, Jiyang Depression. (Burial, thermal and hydrocarbon generation history were modified from Zhang et al., 2009)

5.2 Sources of authigenic clays and quartz in sandstones

Worden and Morad (2003) proposed three possible origins of clay minerals in sandstones: (1) co-deposited with sand grains as sand-sized argillaceous intra- and extra-clasts and as flocculated clays; (2) detrital clay minerals may be incorporated into sandy deposits by

bioturbation and infiltration of muddy waters; (3) diagenetic clay minerals formed by alteration of unstable detrital silicates and by transformation of detrital and precursor diagenetic clay minerals. In this study, the clay minerals occurred mainly as pore-lining and pore-filling cements but no sand-sized argillaceous clasts or flocculated clays were found in sandstones. Therefore, the first origin proposal should be unlikely suitable for the study area.

The clay coats, which are abundant in marginal sandstones, commonly exhibit a combination of thin, honeycomb-like illite/smectite lamina and fibrous or flaky illite ribbons and formed clay cutans arranged tangential to host grains (Fig.16A-C, E) which is the typical characteristic of infiltration-genesis clay coats (Walker et al., 1978). The chalcedony-like pore-filling cements, enriched in primary pores of marginal sandstones, occur as paste colloid suspending with microcrystalline quartz (diameter: 3-20μm) (Fig.16 A, C-E), or kaolinite aggregates coated by cloudy masses (Fig.16 F) under SEM. Both the curved kaolinite aggregates and the flock, smectite-like coats on them demonstrate the feature of flowing structure, which indicates the infiltration origin as well. However, the authigenic clays in the central sandstones are dominated by kaolinite precipitated as relatively isolated patches of euhedral booklets and vermicular aggregates forms, in both secondary (Fig.16G-H, red arrow in Fig.16I) and primary pores (white arrow in Fig.16I).

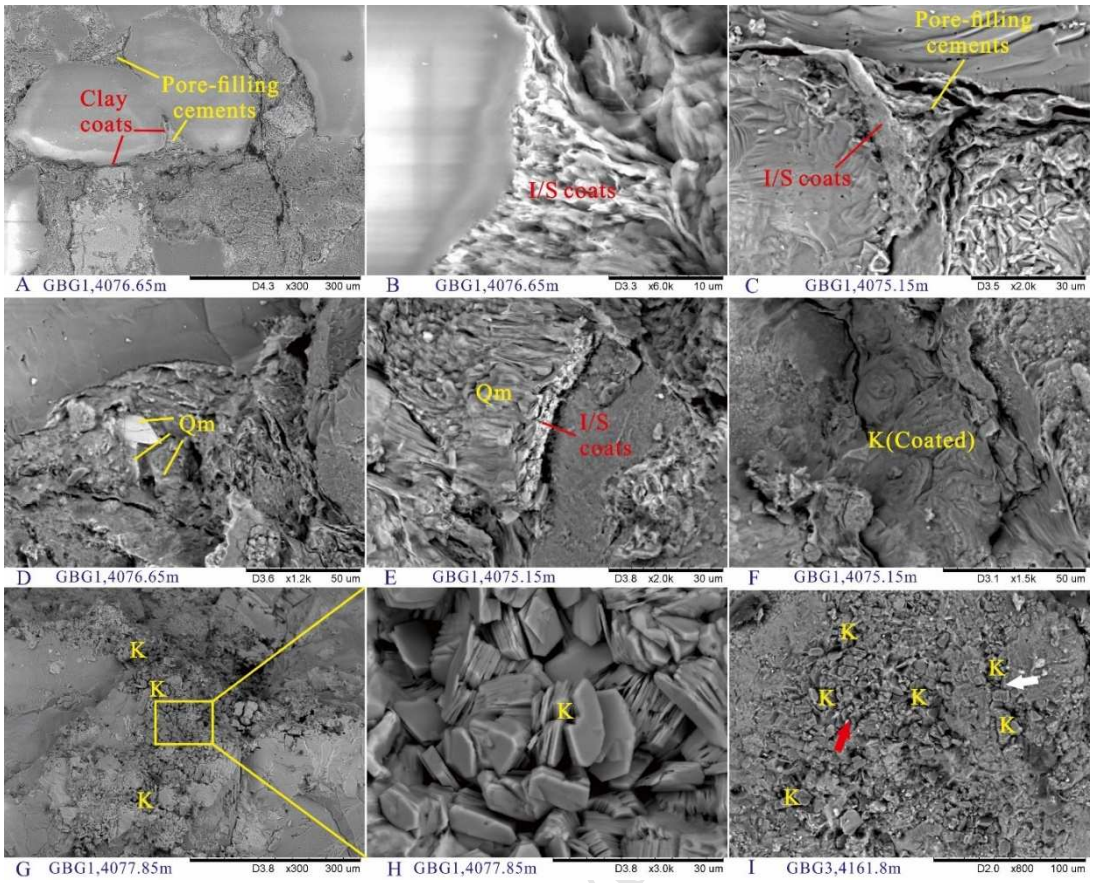

Fig.16 SEM images showing: (A-F) the grain-coating clays and pore-filling cements in marginal sandstones; and (G-I) authigenic clays in dissolution pores of central sandstones. Qm= microcrystalline quartz, K=kaolinite, I/S=illite/smectite mixed layer.

The marginal sandstones have a large number of grain-coating clays with the content ranging from 4.32 % to 24.77% and pore-filling cements varying from 0.05% to 4.28%. Both the content of grain-coating clays and the pore-filling cements show negative correlations with the distance from sandstone samples to the sandstone/mudstone interface (Fig.17A-B). However, these cements occur much less in central sandstones with those two figures ranging stably from 0.28% to 7.79% and from 0% to 0.036% respectively (Fig.17 A-B).

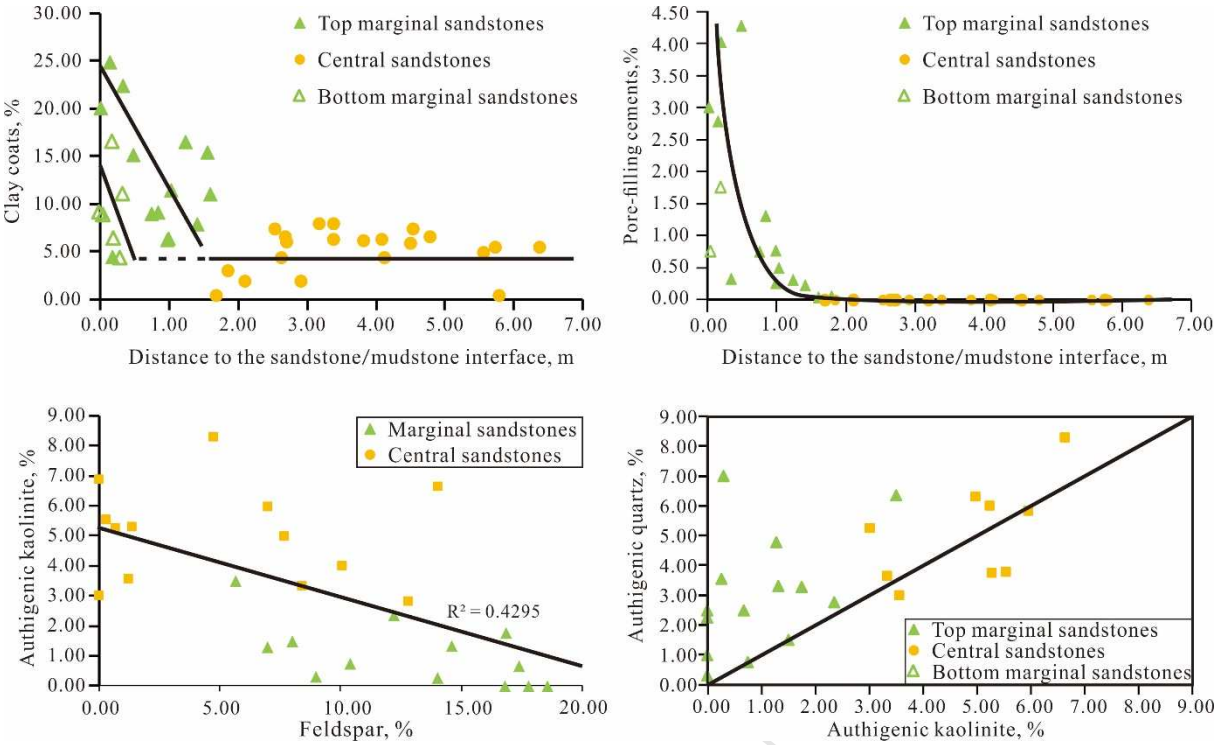

Fig.17 Scatter plots showing the correlation of content between (A) Clay coats and distance to the sand/mud contact; (B) Pore-filing cements and distance to the sand/mud contact; (C) Authigenic kaolinite and feldspar; (D) Authigenic quartz and kaolinite.

The difference is unlikely to be depositional because the marginal and central sandstones in every bed are time-equivalent. Both of them are deposited in the same depositional environment and experienced the same burial and thermal history. The depositional effects can only lead to the mineralogy differences between sandstones in different intervals, but this does not explain the difference in every sandstone bed. The origin of the cements must be post-depositional and external, and the most possible source should be the adjacent mudstone beds. After deposition, porosities of mudstones commonly decline rapidly from nearly 60% to less than 10%-15% (Gluyas and Yuan., 2018; Li et al, 2017). During such a period, large amounts of advective compaction fluids were expelled from mudstones to sandstones (Bjørlykke, 1993; Gluyas et al, 2000; Bjørlykke and Jahren, 2012; Yuan et al., 2015). This

view can perfectly match the deduction above and make it further confirmed.

The authigenic pore-filling kaolinite and the quartz cements are much more abundant in central sandstones than marginal sandstones. Previous studies suggest that the most possible source for authigenic clays and quartz cements should be the dissolution of feldspars within the sandstones, when there is minor pressure dissolution and no external source (Tang et al, 2018; Xi et al, 2015). If both of the precipitation of authigenic pore-filling kaolinite and authigenic quartz were internal sources, a positive correlation should exist between the two, and both the cements should have a negative correlation with the remained feldspar. However, the result turns out to be conflicting.

There is indeed a negative correlation between authigenic kaolinite and remained feldspar in all the sandstones (Fig.17C). However, the positive correlation between authigenic kaolinite and quartz cements is only valid in central sandstones, but fail in marginal sandstones (Fig. 17D). There is much more authigenic quartz than kaolinite in marginal sandstones. All these quantitative data suggest that feldspar dissolution is the internal source for authigenic clays and quartz in both marginal and central sandstones, but authigenic quartz cements in marginal sandstones has part of external source which is most likely the compaction fluid from adjacent mudstones.

5.3 Source of carbonate cements

According to the overview summarized by Morad (2009), carbonate cements form at virtually any stage of diagenesis, from synsedimentary to deep burial. low-Mg calcite, siderite and dolomite cements are precipitated in a range of near-surface settings, especially in subaerial exposure surfaces (caliche crusts, calcretes and dolocretes; see Goudie, 1983;

Wright and Tucker, 1991), areas of shallow meteoric water circulation, sites of syn-sedimentary marine precipitation, as halos around oil or gas seeps, or in areas of near-synsedimentary, microbially-influenced diagenesis. Many mesogenetic settings also are common places to form carbonate cements (Lai et al, 2016), and possible sites of dissolution or alteration of earlier, unstable carbonate cements, carbonate bioclasts and lithoclasts.

In this study, the measured homogenization temperatures (Th) of the aqueous inclusions in carbonate cements are relatively high, ranging from 65°C to 95°C and 100°C to 130°C (Fig.14C-D). This indicates that these carbonate cements were all formed during deep burial, thus they are unlikely to be precipitated in subaerial exposure surfaces, halos around oil or gas seeps, and areas of near-synsedimentary, microbially-influenced diagenesis. However, the Permo-Carboniferous strata underwent significant erosion during the uplift period in Late Triassic, it is a real possibility that the post-Permian meteoric water could have entered the Permian sandstones later, which might be attributed to the precipitation of early-formed dolomites.

This explanation is strengthened by the paleofluid salinity calculated from the freezing temperature (T_f) of aqueous inclusions in carbonate cements. The result shows that the early-formed carbonate cements (with low Th) were precipitated from the pore water with low-salinity, varying from 3.55 to 9.08 wt % NaCl, which indicates that they were precipitated from fresh water. The salinity of inclusions in late carbonate cementation (with higher T_h) are much higher with the range from 10.73 to 22.35 wt %NaCl, which indicates a precipitation in a brine system (Fig.18).

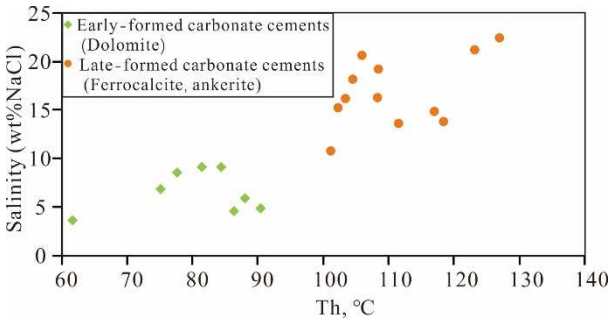

Fig.18 Plot of Th and Salinity data of aqueous inclusions in carbonate cements in Permian sandstones from Gubei Gas field

5.4 Diagenetic sequences

The diagenetic sequences of Permo-Carboniferous in Gubei area are divided into 6 stages (Fig. 19). The principal eogenetic processes experienced in sandstones are compaction, and infiltration of muddy fluids containing a large number of clays and microcrystalline quartz from adjacent mudstones. The infiltration introduced a considerable amount of grain-coating clays and pore-filling cements, which resulted in dramatic reduction of primary porosity and obstruction of subsequent mineral dissolution and quartz overgrowth. Vertically, the infiltration only affected the marginal sandstones within a certain distance (approximately 1.25m at the top and 0.75m at the bottom). Subsequently, the sandstones experienced epidiagenetic stage during the uplift and erosion in the Late Triassic. The process mainly includes the precipitation of quartz cements and kaolinite, the dissolution of feldspars and rock fragments. The mesogenetic features occurred in the second burial process. The diagenesis underwent by the sandstones successively includes the precipitation of dolomite and a little calcite at the beginning of this period, followed by the dissolution of feldspar, rock fragments and dolomite, and the precipitation of quartz cements and kaolinite. Compaction and illitization of smectite continue to occur throughout the entire burial process. Although

the tectonic uplift occurred again in the Middle to Late Cretaceous, it is unlikely that epigenetic stage could be experienced by Permo-Carboniferous sandstones during this stage, owing to the thick Mesozoic sediments. However, the uplift resulted in a decrease in CO_2 partial pressure and a large amount of carbon dioxide separation from the pore water, thus led to the precipitation of late carbonate cements, such as ferrocalcite and ankerite. In the duration of third burial process, the diagenetic processes were dominated by (1) compaction, (2) illitization of smectite, and (3) a little mineral dissolution, which was caused by CO_2 produced by decarboxylation of organic acids, and the precipitation of quartz cements and kaolinite associated with the dissolution.

Some mesogenetic features, such as feldspar dissolution and the precipitation of kaolinite and authigenic quartz (especially quartz overgrowth), were far less present in the marginal sandstones. This is due to the inhibited dissolution of grains by clay coats and the cramming of primary pores by pore-filling cements. Furthermore, the limitation of pores resulting from the same reason above also account for the fact that early-formed dolomites mainly present as mineral replacement in marginal sandstones.

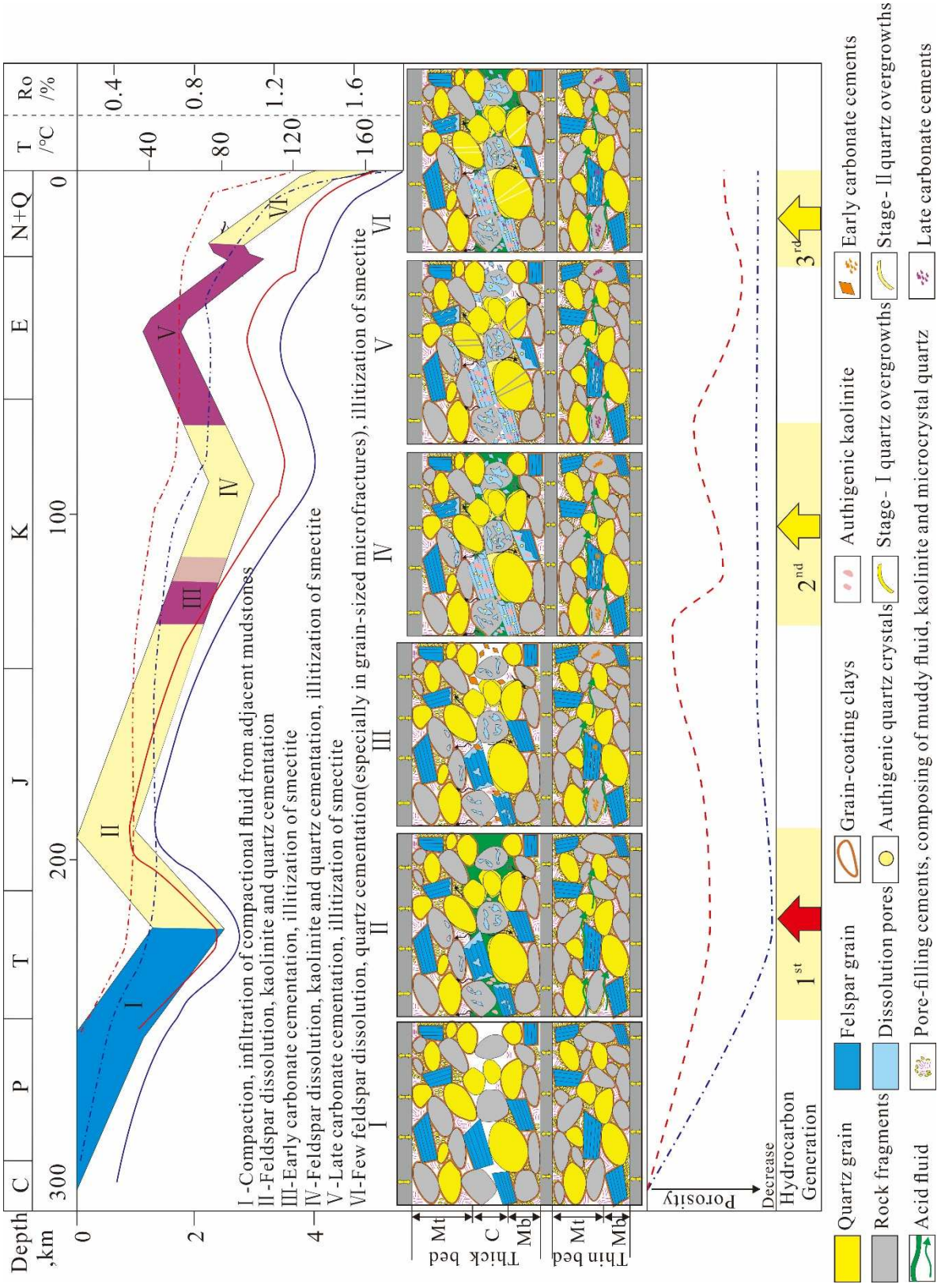

Fig.19 *Diagram showing the coupling relationship of burial, thermal, hydrocarbon generation, diagenetic and speculative reservoir quality evolution history of the Permian sandstones in Gubei area (Burial and thermal history were modified from Zhang et al., 2009).*

5.5 Hydrocarbon filling history

Three periods of hydrocarbon generation of Permo-Carboniferous source rocks were determined according to the analysis of thermal history and hydrocarbon generation history. Among them, the Yanshan period and Xishan period are the main periods with the conversion rate of methane ranging from 7.73%-9.78%, 21.05%-48.03% respectively (Zhang et al, 2009). The T_h of the aqueous inclusions associated with hydrocarbon-bearing fluid inclusions in sandstones was examined and the exact dating of hydrocarbon filling was carried out based on the combined analysis of homogenization temperature and reservoir burial heating history (the analysis method refers to Jiang et al, 2016). The results show that the hydrocarbon filling mainly occurred in two stages: the Late Cretaceous and the Neogene (Table 2).

Table 2 Thermometry data of aqueous inclusions associated with hydrocarbon-bearing fluid inclusions in Permian sandstones from the Gubei Gas field (The dates were acquired by the combined analysis of homogenization temperature and reservoir burial heating history)

Well	Strata	Depth, m	Aqueous inclusions associated with hydrocarbon-bearing fluid inclusions Th ℃ （average）	Age for inclusions formation, Ma (Geological time)
Y135	P_{1sh}	4892.3	165~200(195.5)	8.5-6.6 (Mid Nm)
GBG1	P_{1sh}	4403.9	98~149(126.5); 161~163(162)	115-98(Late K); 10.3-8.1 (Early Nm)
GBG3	P_{2x}	4090	106~108(107); 137~145(141)	105-103(Late K); 11.3-3.4(Nm)
B930	P_{1x}	3623	114~139 (123.46)	108.3-95(Late K)
B930	P_{1x}	3625	111~126 (122.2); 145~159 (152.5)	109-100(Late K); 10.7-2.45(Nm)
B930	P_{1x}	3674.7	117~129 (122.6)	113.8-98.3(Late K)
Y132	P_{1x}	3598.5	118 (118); 138~152 (140.3)	96.3 (Late K); 3.1-0(Late Nm to date)
Y132	P_{1x}	3599.5	118~127 (120.6); 136~148 (140.5)	18.6-9.9 (Mid Ng-early Nm); 3.16-0 (Late Nm to date)
Y132	P_{1x}	3598	106~125 (116.6)	20.3-16.8(Mid Ng)
Y132	P_{1x}	3599	109~136 (125.2)	11.9-6.7(Early Nm)

Y134	P_{1x}	3507	120~130 (124)	100.5-95(Late K)
Y136	P_{1x}	3696	115~135 (123.3)	106-95 (Late K)
Y136	P_{1x}	3708	123~125 (124.7); 155~167 (160.5)	101.2 (Late K); 3.3-0 (Late Nm to date)
Y136	P_{1x}	3715.2	164~177 (170.6)	2.5-0 (Late Nm to date)
GBG2	P_{1sh}	3692.8	117~141 (130.4)	16.8-0 (Mid Ng to date)
GBG2	P_{2w}	3546.9	124~142 (133.4)	12-0 (Early Nm to date)

5.6 Coupling relationship among diagenesis, reservoir quality evolution and the hydrocarbon differential filling

The compaction and cementation are two main processes reducing reservoir quality during burial diagenesis (Ehrenberg 1989; Gluyas and Cade 1997). The contribution of compaction and cementation on porosity reduction in this study was quantitatively characterized by the "intergranular porosity-intergranular volume-total cement diagram" proposed by Houseknecht (1987). The initial porosity was set as 40% (Tang et al 2018). The result shows that the proportions of initial porosity reduced by compaction in marginal and central sandstones reach up to an average of 61% and 70.15%, respectively, while the percentages reduced by cementation are 38.27% and 28.1% individually (Fig.20). This indicates that cementation exerted more contributions to primary porosity loss in the marginal sandstones than in the central ones, which might be due to the reason that the clay output from mudstones significantly occupied the pore space. For the porosity enhancement processes, secondary pores, especially mineral dissolution pores, are the main spaces for hydrocarbon storage, and the dissolution of minerals including feldspar, rock fragments and carbonate cements are the major mechanism for the improvement of reservoir quality (Lai et al, 2017a; Mahmic et al, 2018).

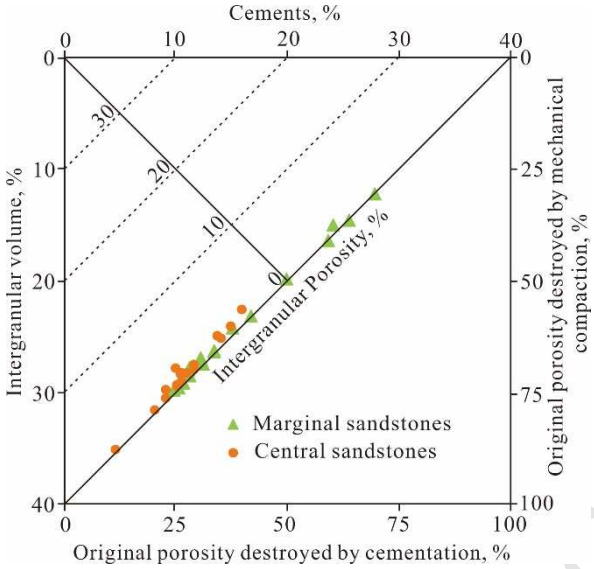

Fig.20 Intergranular volume versus cement with the importance of compaction/cementation on reducing porosity in marginal and central sandstones. The diagram refers to Houseknecht 1987.

Characteristics of speculative porosity evolution were shown in the Fig. 20. For marginal sandstones, the initial porosity was dramatically reduced by the mass output from mudstone. Only a small amount of porosity increased in the subsequent dissolution processes by acids due to the reason that the clay coats and pore-filling cements in sandstones are effective for inhibiting dissolution of grains. With regard to the central sandstones, more initial porosity was remained before the first dissolution process in the uplift period because the burial depth was only around 2200m and hardly affected by the mass input. This provided favorable acid transport access and fluid-grain contact conditions for later dissolution processes. Therefore, relatively larger number of acid-genetic secondary pores were formed during the subsequent diagenesis, which led to the significant enhancement of porosity (ranging from 3.8 %-12.00%).

Two major hydrocarbon generation stages, the Late Cretaceous and the Neogene, both occurred in the stages of porosity enhancement of the sandstones (Fig.19). However,

porosities of the marginal sandstones are much lower than the central sandstones, which indicates higher filling resistance of hydrocarbon filling in the marginal sandstones. For the gas generated during the same period, the driving force filling into the sandstones is considered to be the similar, and the D-value between the driving force and resistance is the main dynamic mechanism that determines the state of hydrocarbon filling (Pang et al, 2014). Therefore, central sandstones are more conducive to the gas filling than marginal sandstones. This conclusion was confirmed by the GOI (Lisk and Eadington, 1994) examination. The GOI is defined as Grains containing Oil Inclusions, but it is used to represent the grains containing hydrocarbon-bearing inclusions in this study. The result shows that central sandstones demonstrate higher GOI value ranging from 9%-19.65% than marginal sandstones with just 0%-3.6% (Fig.21).

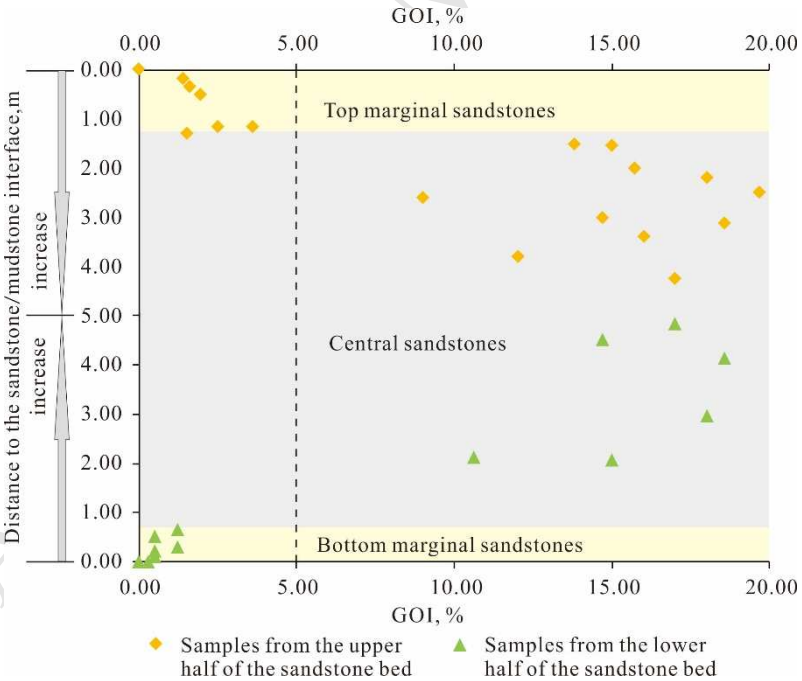

Fig.22 Plot showing correlation between GOI value and the distance to sandstone/mudstone contact

Conclusions

(1) The natural gas mainly accumulated in the P_2k and P_2w members of Permian, which

have the highest and the most stable net to gross ratio values; all the natural gas occurred in the sandstone beds with thickness over 1.9 m.

(2) The porosity of the Permo-Carboniferous sandstones in Gubei area are of considerable heterogeneity. For every single bed, two porosity transitional zones exist on the top and bottom of the bed with thicknesses of 1.25m and 0.75m respectively; the porosities in the transitional zones show a positive correlation with the distance to the sandstone/mudstone contact.

(3) The mudstone beds interbedded and associated with the sandstones have had important influence on the reservoir quality of the sandstones through providing diagenetic fluids capable of cementation and considerable porosity reduction, and the impact is greater for sandstones at the margin of sandstone beds than for the central ones. The thickness of these infiltrated zones reaches up to 1.25 m and 0.75m at the top and bottom of every bed respectively, leading thin sandstone beds with thickness of approximately 2m to be tightly cemented totally.

(4) The multi-staged diagenetic processes lead to three porosity reduction stages and three porosity enhancement stages occurring alternately. The hydrocarbon filling mainly occurred in two stages: the Late Cretaceous and the Neogene, corresponding to the porosity enhancement stages. The difference of reservoir quality between marginal and central sandstones led to the differential filling of the natural gas. The central sandstones of thick beds within the effective acid-affected area can be potential effective reservoirs.

(5) The observations made on this interbedded sequence of mudstones with sandstones differential reservoir quality and hence gas saturation has important implications for exploring

areas with similar reservoirs be it for conventional or shale gas opportunities.

Acknowledgements

The authors gratefully acknowledge the financial support from the China National major projects (Item No.2016ZX05006-007). Thanks are also given to the Shengli Oilfield Company of Sinopec provided all the related geological and experimental data.

References

Ajdukiewicz, J. M., and Larese, R. E., 2012. How clay grain coats inhibit quartz cement and preserve porosity in deeply buried sandstones: Observations and experiments. AAPG Bulletin. 96, 2091-2119.

Bjørlykke, K., 1993. Fluid flow in sedimentary basins. Sediment. Geol. 86, 137-158.

Bjørlykke, K., Jahren, J., 2012. Open or closed geochemical systems during diagenesis in sedimentary basins: constraints on mass transfer during diagenesis and the prediction of porosity in sandstone and carbonate reservoirs. AAPG Bull. 96(12), 2193-2214.

Bjørlykke, K., 2014. Relationships between depositional environments, burial history and rock properties. Some principal aspects of diagenetic process in sedimentary basins. Sediment. Geol. 301, 1-14.

Crossey, L.J, Frost, B.R, Surdam, R C., 1984. Secondary Porosity in Laumontite-Bearing Sandstones: Part 2. Aspects of Porosity Modification.

Dutton, S.P., Loucks, R.G., 2010. Reprint of: Diagenetic controls on evolution of porosity and permeability in lower Tertiary Wilcox sandstones from shallow to ultradeep (200–6700 m) burial, Gulf of Mexico Basin, USA. Marine and Petroleum Geology. 27(8), 1775-1787.

Ehrenberg, S., Nadeau, P.,1989. Formation of diagenetic illite in sandstones of the Garn Formation, Haltenbanken area, mid-Norwegian continental shelf. Clay Miner. 24(2), 233-53.

Gluyas, J., Cade, C.A., 1997. Prediction of porosity in compacted sands. In: AAPG memoir: reservoir quality prediction in sandstones and carbonates. 69, 19–27.

Gluyas, J., Garland, C., Oxtoby, N.H., Hogg, A.J.C., 2000. Quartz cement: the Miller's tale.

Journal Recommendation service. 29, 199-218.

Gluyas, J.G., Yuan, G.H., 2018. Diagenesis. In: Sorkhabi R. (eds) Encyclopedia of Petroleum Geoscience. Encyclopedia of Earth Sciences Series. Springer, Cham.

Goudie, A. S., 1983. Calcrete, in A. S. Goudie, and K. Pye, eds., Chemical Sediments and Geomorphology: Precipitates and Residua in the Nearsurface Environment: London, Academic Press. 93-132.

Houseknecht, D.W., 1987. Assessing the relative importance of compaction processes and cementation to reduction of porosity in sandstones. AAPG Bull.71(6), 633–42.

Jiang, Y.L., Fang L., Liu J.D., Hu, H.J., Xu, T.W., 2016. Hydrocarbon charge history of the Paleogene reservoir in the northern Dongpu Depression, Bohai Bay Basin, China. Petroleum Science. 13(4): 625-641.

Jiang, Y.L., Liu, H., Li, Z.L., 2010. Effective migration pathways of deep gas in Bonan and Gubei area, Jiyang Depression. Geological Review. 56(4), 525-530.

Kharaka, Y.K., Hull, R.W., Carothers, W.W., 1985. Water-rock interactions in sedimentary basins.

Krynine, P.D., 1949. Section of geology and mineralogy: the origin of red beds. Transactions of the New York Academy of Sciences. 11(3 Series II), 60-68.

Lai, J., Wang, G., Ran, Y., Zhou, Z., Cui, Y., 2016. Impact of diagenesis on the petrophysical properties of tight oil reservoirs: the case of Upper Triassic Yanchang Formation Chang 7 oil layers in Ordos Basin, China. J. Pet. Sci. Eng. 145, 54-65.

Lai, J., Wang, G.W., Cai, C., Fan, Z.Y., Wang, S.C., Chen, J., Luo, G.X., 2017a. Diagenesis and reservoir quality in tight gas sandstones: The fourth member of the Upper Triassic Xujiahe Formation, Central Sichuan Basin, Southwest China. Geological Journal. 53(2),629-646.

Lai, J., Wang, G., Chai, Y., Xin, Y., Wu, Q., Zhang, X., and Sun, Y., 2017b. Deep burial diagenesis and reservoir quality evolution of high-temperature, high-pressure sandstones: Examples from Lower Cretaceous Bashijiqike Formation in Keshen area, Kuqa depression, Tarim basin of China. AAPG Bulletin, 101(6): 829-862.

Lai J., Wang G., Wang S., Cao J., Li M., Pang X., Zhou Z., Fan X., Dai Q., Yang L., He Z., Qin Z. 2018. Review of diagenetic facies in tight sandstones: Diagenesis, diagenetic

minerals, and prediction via well logs. Earth-Science Reviews, 185, 234-258.

Li, C., Zhang, L.K., Luo, X.R., Zhang, L.Q., Hu, C.Z., Qi, Y.K., Lei, Y.H., Cao, B.F., Cheng, M., Yu, Y.X., 2017. Calibration of the mudrock compaction curve by eliminating the effect of organic matter in organic-rich shales: Application to the southern Ordos Basin, China. Marine & Petroleum Geology. 86:620-635.

Li, J.D., Xu, S.T., Yang, Y.E., Ke, M.W., Zhao, Q., 2015. Forming condition analysis of Hugu 2 gas reservoir in Dongpu Depression. Fault-Block Oil&Gas Field. 22(4), 450-453.

Lin, W., Li, Z., Li, J.Y., Xu, X.Y., 2007. Genetic types and distribution pattern of natural gases in Gubei buried-hills, Jiyang Depression. Oil & Gas Geology. 28(3), 419-426.

Lisk, M., Eadington, P.J., 1994. Oil migration in the Cartier Trough, Vulcan Sub-basin. In: Purcell, P.G., Purcell, R.R. (Eds.), The Sedimentary Basins of Western Australia, Proceedings of the West Australian Basins Symposium, Perth, WA, pp. 301–312.

Liu, J. Study on reservoir geology of coal-formed gas in Pre-tertiary in Gubei deeply buried hill. China University of Petroleum (East China), pp. 10-12.

Liu, N., Qiu, N.S., Chang, J., Shen, F.Y., Wu, H., Lu, X.S., Wang, Y.J., Jiao, Y.X., Feng, Q.Q., 2017. Hydrocarbon migration and accumulation of the Suqiao buried-hill zone in Wen'an Slope, Jizhong Subbasin, Bohai Bay Basin, China. Marine & Petroleum Geology. 86, 512-525.

Mahmic, O., Dypvik, H., Hammer, E., 2018. Diagenetic influence on reservoir quality evolution, examples from Triassic conglomerates/arenites in the Edvard Grieg field, Norwegian North Sea. Marine & Petroleum Geology. 93:247-271.

Morad, S. (Ed.), 2009. Carbonate cementation in sandstones: distribution patterns and geochemical evolution (Vol. 72). John Wiley & Sons.

Morad, S., Al-Ramadan, K., Ketzer, J.M., De Ros, L.F., 2010. The impact of diagenesis on the heterogenity of sandstone reservoirs: A review of the role of depositional facies and sequence stratigraphy. AAPG Bull. 94 (8), 1267-1309.

Pang, X.Q., Huang H.D., Lin C.S., Zhu, X.M., Liao, Y., Chen, J.F., 2014. Formation distribution exploration and resource/reserve assessment of superimposed continuous gas field in Marsel exploration area, Kazakhstan. Acta Petrolei Sinica. 35(6),1012-1056.

Peng, Z.M., Wu, Z.P., Peng, S.M., 2010. Basin superposition characteristics of Mesozoic and

Cenozoic and natural gas exploration prospect of Upper Paleozoic in the eastern North China. Journal of China University of Petroleum. 34(2), 1-7.

Robinson, A., Gluyas, J., 1992. Duration of quartz cementation in sandstones, North Sea and Haltenbanken Basins. Mar. Pet. Geol. 9, 324-327

Surdam, R.C., Boese, S.W., Crossey, L.J.,1984. The chemistry of secondary porosity: Part 2. Aspects of porosity modification.

Surdam, R.C., Crossey, L.J., Hagen, E.S., Heasler, H.P.,1989. Organic-inorganic interactions and sandstone diagenesis. AAPG Bulletin. 73(1), 1-23.

Surdam, R.C., Wolfbauer, C.A.,1975. Green River Formation, Wyoming: a playa-lake complex. Geological Society of America Bulletin. 86(3),335-345.

Tang, L.X., Gluyas, J., Jones, S., Bowen, L., 2018. Diagenetic and geochemical studies of the Buchan Formation (Upper Devonian) in the Central North Sea. Petroleum Science. 15(2), 211-229.

Taylor, T.R., Giles, M.R., Hathon, L.A., Diggs, T.N., Braunsdorf, N.R., Birbiglia, G.V., Kittridge, M.G., Macaulay C.I., Espejo I.S., 2010. Sandstone diagenesis and reservoir quality prediction: Models, myths, and reality. AAPG bulletin. 94(8), 1093-1132.

Ulmer-Scholle, D.S., Scholle, P. A., Schieber, J., Raine, R. J., 2014. Diagenesis: Introduction and Quartz & Silica Cements. 245-264.

Walker, T. R., Waugh, B., and Crone, A. J., 1978, Diagenesis in first cycle desert alluvium of Cenozoic age, southwestern United States and northwestern Mexico: GSA Bulletin. 89, 19-32,

Worden, R.H., Morad, S., 2003. Clay mineral cements in sandstones. Blackwell Pub. 34, 3-41.

Wright, V. P., and Tucker, M. E., 1991. Calcretes: An introduction, in V. P. Wright, and M. E. Tucker, eds., Calcretes (International Association of Sedimentologists Reprint Series 2): Oxford, UK. Blackwell Publishing Ltd. 1-22.

Xi, K.L., Cao, Y.C., Jaren, J., Zhu, R., Bjørlykke, K., Zhang, X., 2015. Quartz cement and its origin in tight sandstone reservoirs of the Cretaceous Quantou formation in the southern Songliao Basin, China. Mar. Pet. Geol. 66, 748-763.

Yu, X.H., Li, S., Li, S.,2018. Clastic Hydrocarbon Reservoir Sedimentology. Springer. 275-280.

Yuan, G.H., Gluyas, J.G., Cao, Y.C., Oxtoby, N.H., Jia, Z.Z., Wang Y.Z., Xi, K.L., Li, X.Y.,2015. Diagenesis and reservoir quality evolution of the Eocene sandstones in the northern Dongying Sag, Bohai Bay Basin, East China. Marine and Petroleum Geology. 62, 77-89.

Zhang, S.W., Zhang, L.Y., Li, Z., 2009. Analysis of Accumulation Process of Coal-Formed Gas in Gubei Buried Hill of Jiyang Depression. Natural Gas Geoscience.20(5), 670-677.

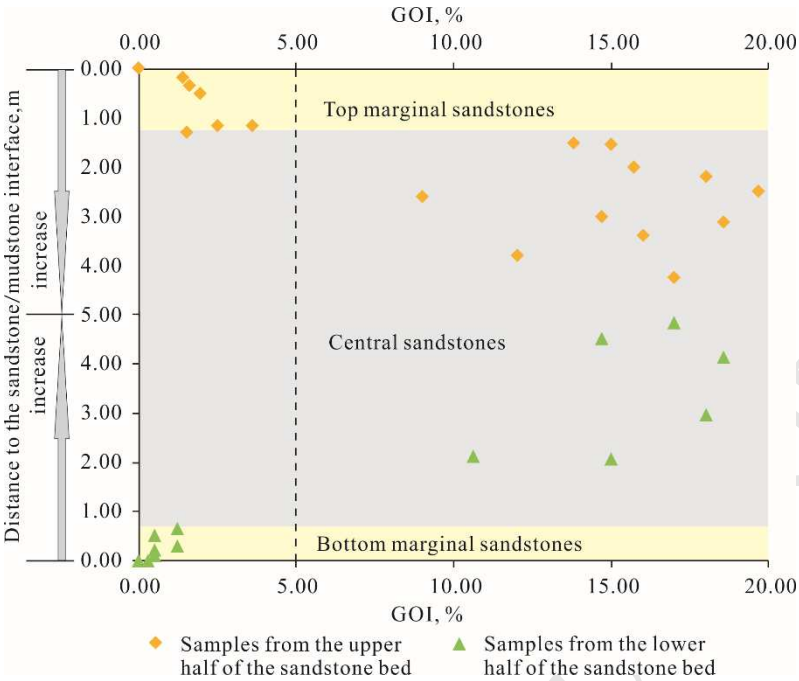

Fig.21 Plot showing correlation between GOI value and the distance to sandstone/mudstone contact

Highlights:

1. Identification of the porosity transitional zones at the top and bottom marginal zones of every single bed.

2. Confirmation of the influence of the interbedded mudstone beds on the sandstone reservoir quality through providing diagenetic fluids capable of cementation.

3. The differential diagenesis between marginal and central sandstones caused by the mass input are the key reasons for the differential filling of hydrocarbon in sandstone beds.

4. The central sandstones of thick beds within the effective acid-affected area can be potential effective reservoirs.